

AD/A-001 242

EXPLOSION HAZARDS ASSOCIATED WITH SPILLS  
OF LARGE QUANTITIES OF HAZARDOUS  
MATERIALS. PHASE I

C. D. Lind

Naval Weapons Center

Prepared for:

Coast Guard

October 1974

DISTRIBUTED BY:

**NTIS**

National Technical Information Service  
U. S. DEPARTMENT OF COMMERCE

Technical Report Documentation Page

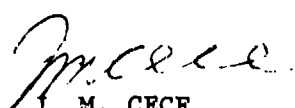
1. Report No. CG-D-30-75	2. Government Accession No.	3. Recipient's Catalog No. <i>ADA-001 242</i>	
4. Title and Subtitle Explosion Hazards Associated with Spills of Large Quantities of Hazardous Materials Phase I		5. Report Date October 1974	
		6. Performing Organization Code	
7. Author(s) C. D. Lind		8. Performing Organization Report No.	
9. Performing Organization Name and Address Department of the Navy Naval Weapons Center China Lake, California 93555		10. Work Unit No. (TRAIS) 3126.1	
		11. Contract or Grant No. DOT -CG-34,095-B	
12. Sponsoring Agency Name and Address Commandant (G-DST) U. S. Coast Guard Headquarters Washington, D.C. 20590		13. Type of Report and Period Covered  Interim Report	
		14. Sponsoring Agency Code	
15. Supplementary Notes			
16. Abstract <p>This report documents the results of Phase I of a program whose object is to quantify the explosion hazards associated with spills of large quantities of hazardous material such as liquified natural gas (LNG), liquified petroleum gas (LPG), or ethylene. The principal results are (1) a phenomenological description of a spill, (2) an examination of the detonation properties of methane, (3) a qualitative theory of non-ideal explosions, and (4) a plan for Phase II of the study.</p>			
17. Key Words Explosion Hazard Spills Hazardous Materials		18. Distribution Statement Document is available to the public through the National Technical Information Service, Springfield, Va. 22151	
19. Security Classif. (of this report) Unclassified	20. Security Classif. (of this page) Unclassified	21. No. of Pages <i>63</i>	22. Price <i>\$4.25-2.25</i>

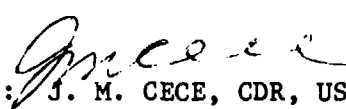
Reproduced by  
NATIONAL TECHNICAL  
INFORMATION SERVICE  
U S Department of Commerce  
Springfield VA 22151


18 OCT 1974

The work reported herein was accomplished for the U. S. Coast Guard's Office of Research and Development, Marine Safety Technology Division, as part of its program in Cargo Safety Technology.

The contents of this report reflect the views of the Author, who is responsible for the facts and the accuracy of the data presented herein. The contents do not necessarily reflect the official views or policy of the Coast Guard. This report does not constitute a standard, specification, or regulation.

  
Reviewed by: J. M. CECE  
Project Officer

  
Submitted by: J. M. CECE, CDR, USCG  
Chief, Marine Safety Projects Branch

  
Released by: W. D. MARKLE, JR., CAPT, USCG  
Chief, Marine Safety Technology Division  
Office of Research and Development  
U. S. Coast Guard Headquarters  
Washington, D. C. 20590

EXPLOSION HAZARDS ASSOCIATED WITH  
SPILLS OF LARGE QUANTITIES OF  
HAZARDOUS MATERIALS

PHASE I

by

C. D. Lind

## CONTENTS

Introduction . . . . .	3
Scenario of a Possible Accident . . . . .	3
Initial Conditions . . . . .	3
Cloud Formation and Dispersion . . . . .	3
Ignition and Detonation . . . . .	4
Blast Wave and Damage . . . . .	4
Variations of Accident Conditions Investigated . . . . .	4
Spill Size . . . . .	4
Variations in Atmospheric Conditions . . . . .	4
Point of Ignition . . . . .	5
Explosive Behavior — Methane/Air Mixtures . . . . .	5
Ideal Detonation . . . . .	5
Detonation Tube Experiments . . . . .	5
Professor Williams' Formulation . . . . .	5
Vapor Cloud Explosion Study . . . . .	9
Appendix A. Calculation of Methane Vapor Cloud Generation and Dispersion . . . . .	17
Appendix B. Qualitative Theory of Non-Ideal Explosions . . . . .	31
Appendix C. Annotated Bibliography . . . . .	51
Bibliography . . . . .	55

## ABSTRACT

This report documents the results of Phase I of a program whose object is to quantify the explosion hazards associated with spills of large quantities of hazardous material such as liquified natural gas (LNG), liquified petroleum gas (LPG), or ethylene. The principal results are (1) a phenomenological description of a spill, (2) an examination of the detonation properties of methane, (3) a qualitative theory of non-ideal explosions, and (4) a plan for Phase II of the study.

## INTRODUCTION

The nation's navigable waters provide an efficient means of transporting large quantities of bulk materials. Hazardous materials such as ethylene, butadiene, and liquified petroleum gases (LPG) are commonly shipped in liquid form in large quantities. In general, the operation becomes more economical as the quantity that can be shipped at one time is increased. Thus, the tendency has been to increase the size of the shipping container, leading to the recent advent of the super tanker for shipping liquified natural gas (LNG). Unfortunately, as the quantity of material shipped at one time increases, so does the potential hazard associated with accidental spillage of the material. The significance of the larger quantities is that we now have the potential for accidentally forming extremely large vapor clouds whose burning characteristics are not understood.

## SCENARIO OF A POSSIBLE ACCIDENT

In order to become familiar with the scale of possible accidents, a hypothetical spill was investigated. The size of the spill chosen is somewhat arbitrary and represents an intermediate size (the capacity of one compartment of an existing tanker, the Descartes). Current construction and plans are for 125,000 m<sup>3</sup> ships. In most cases, assumptions were made which makes the outcome a worse case. The calculations of pool spread and atmospheric dispersion were made by the method of reference.<sup>1</sup>

## INITIAL CONDITIONS

An LNG tanker with 50,000 m<sup>3</sup> LNG in five compartments moors 3,500 meters upwind from shore at an offshore tanker unloading terminal. The wind velocity is 2.24 m/sec, temperature 21°C, and relative humidity 75%. The atmosphere is very stable due to an inversion (horizontal dispersion coefficient - Pasquil C; vertical dispersion coefficient - Singer and Smith D).

## SPILL

A collision occurs between the tanker and another ship. The collision is at the aft compartment and releases 10,000 m<sup>3</sup> of LNG onto the water. Although ignition sources occur at the point of impact, a sustaining reaction does not take place. The pool of LNG spreads to a maximum diameter of 400 meters in 5 minutes. The boil-off reaches a maximum of 26,000 kg/sec; however, the downwind drift is only 5,000 kg/sec. Therefore, a vapor accumulation occurs over the spill point of  $3.5 \times 10^6$  kg in a volume 400 meters in diameter and 9 meters high.

## CLOUD FORMATION AND DISPERSION

The vapor accumulation over the spill point is more dense than the surrounding air because of its low temperature. It spreads due to gravity and moves downwind as

---

<sup>1</sup>Spills of LNG on Water-Vaporization and Downwind Drift of Combustible Mixtures, by G. W. Fieldbauer, et. al., Esso Research and Engineering Company, Report No. EF61E-72 (1972). Released by the American Petroleum Institute, Re Z32, March 1973.

Preceding page blank

it warms and mixes with air until its density equals air density. At the end of the gravity spread phase the cloud has moved 500 meters downwind, is 2,000 meters wide, 9 meters high, and has an average concentration of 22%. Twelve and one-half minutes have passed since time of spill. The cloud then evolves due to wind drift and dispersion. At the end of 35 minutes from spill time the front of the cloud (of concentration above 5%) has reached the shore (3,500 meters from spill point). The volume of cloud with a concentration above 5% has a maximum width of 2,000 meters, height of 18 meters, and length of 2,000 meters.

## IGNITION AND DETONATION

An ignition now occurs at some point within the cloud, perhaps from a small craft. The ignition starts a flame front moving through the cloud which accelerates and a transition to a detonation occurs. The properties of the detonation wave are: pressure — 14 bars, velocity — 1,700 m/sec, temperature — 2,500°K. It is assumed that the entire cloud detonates.

## BLAST WAVE AND DAMAGE

The detonation wave in the cloud produces a blast wave in the air which expands and decays as it moves over the land. The amount of damage done by the blast wave depends on the population density and the density of damagable structures. The damage levels are as follows: 50% fatalities to exposed personnel within 200 meters; 90% ear drum damage to exposed personnel within 300 meters; and 100% damage to frame structures within 450 meters, 50% damage to frame structures within 700 meters, and glass breakage to a distance of 4,000 meters. Distances are from the edge of the cloud.

## VARIATIONS OF ACCIDENT CONDITIONS INVESTIGATED

### SPIII SIZE

The 10,000 m<sup>3</sup> spill size used in the example was chosen because this is the capacity of one of the compartments of an existing LNG tanker (the *Descartes*). Two other spill sizes were investigated; 4,000 m<sup>3</sup> and 50,000 m<sup>3</sup>. Results of these calculations and the method of calculation are shown in Appendix A.

### VARIATIONS IN ATMOSPHERIC CONDITIONS

The wind speed chosen (2.24 m/sec) represents a worse case condition. Lower speeds lead to a localization of the cloud and higher speeds produce greater dispersion and thus a smaller volume of over 5% concentration. Less stable atmospheric conditions also lead to smaller cloud volume due to turbulence and greater vertical mixing. Air temperature has a minor effect—higher temperatures cause thinner, wider clouds; lower temperatures cause thicker, narrower clouds.



## POINT OF IGNITION

The possibility exists that an ignition could occur at the point of spill before the cloud formed. Since the major part of the fuel would be at a concentration above the upper flammability limit, a diffusion flame would develop. This outcome was not investigated since it is the subject of another study. Ignition at point of spill is not a certainty, as demonstrated by NWC experience with explosively opening tanks of flammable fuels without ignition.

## EXPLOSIVE BEHAVIOR - METHANE/AIR MIXTURES

### IDEAL DETONATION

Ideal detonation properties of methane/air mixtures have been calculated. The computer code used assumes chemical equilibrium in the detonation wave and calculates detonation pressure, temperature, and velocity as a function of initial composition. The calculations do not determine if the mixture will detonate but only predict the properties of the detonation if it occurs. The results of the calculations are shown in Figures 1, 2 and 3. The figures also show the experimentally determined lower flammability limit (LFL)<sup>2</sup>, upper flammability limit (UFL)<sup>2</sup>, and the calculated stoichiometric compositions.

### DETONATION TUBE EXPERIMENTS

An attempt was made to measure the detonation and limits of methane/air mixtures. The experiments were carried out in a 60 centimeter diameter, 180 centimeter long steel tube. In use, an explosive booster is placed at one end of the tube, both ends are covered with polyethylene film, and a known amount of methane is introduced. After mixing, the explosive booster is detonated and the results are sensed by transducers in the side of the tube. Results indicated that no reaction was observed with a small booster (5 grams tetryl), and with a large booster (90 grams sheet explosive) pressures and velocities were far below the calculated values. Methane/air mixtures were tested in the composition range of 5-13% by volume methane. The detonation limits appear to be 6-12.5%, although with the low extent of reaction observed it is difficult to accurately determine the limits. Velocities measured were 950 to 1,050 m/sec and pressures from 5 to 8 bars. The pressure traces showed a complex wave pattern indicating a non-ideal detonation.

### PROFESSOR WILLIAMS' FORMULATION

Because of the doubts raised by the detonation tube experiments and other evidence, Professor F. A. Williams was asked to make a theoretical study of the burning reaction and the transition from burning to detonation. Professor Williams

---

<sup>2</sup>*Flammability Characteristics of Combustible Gases and Vapors*, by G. Zabetakis, Bureau of Mines, Bulletin 627, 1965.

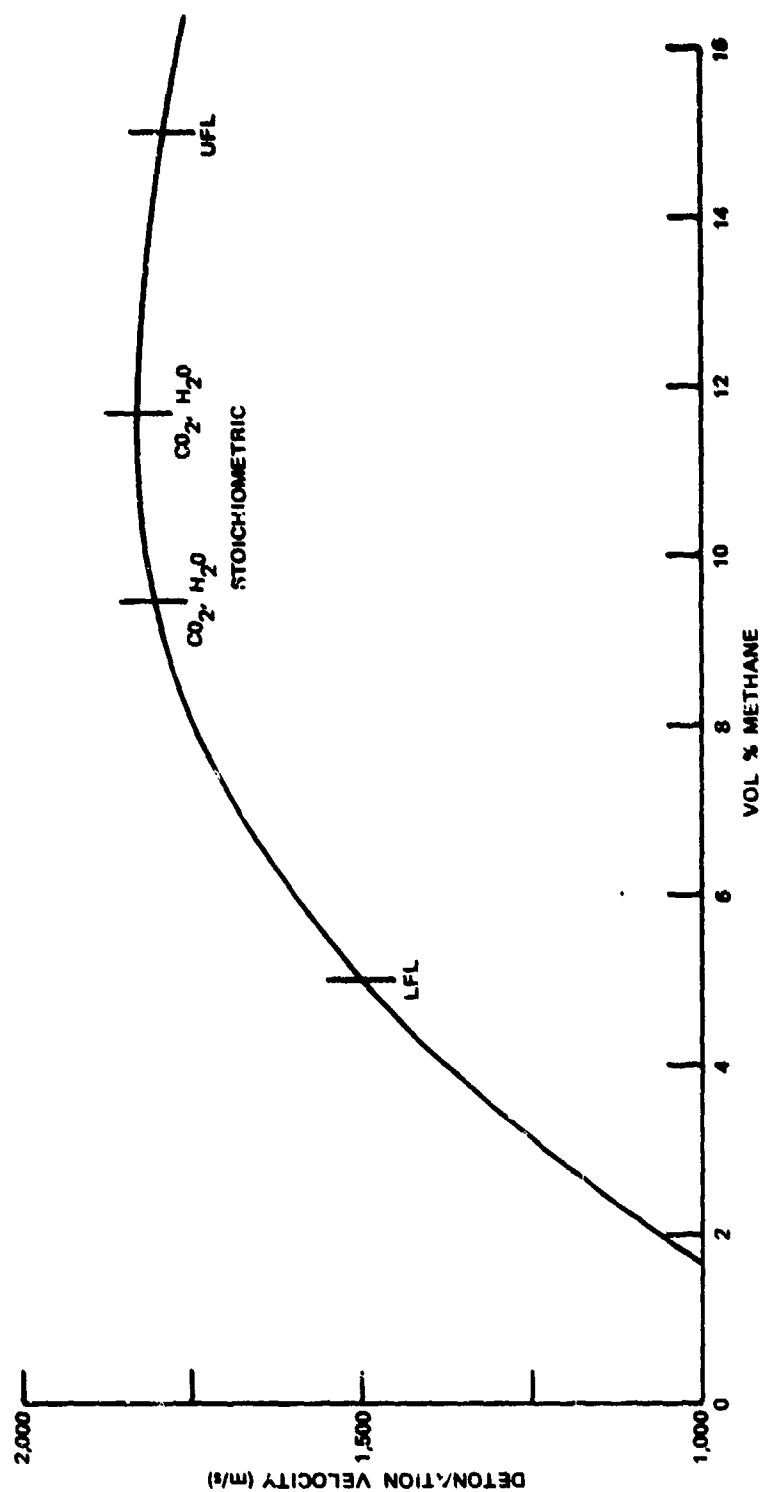


FIGURE 1. Calculated Detonation Velocity, Methane/Air.

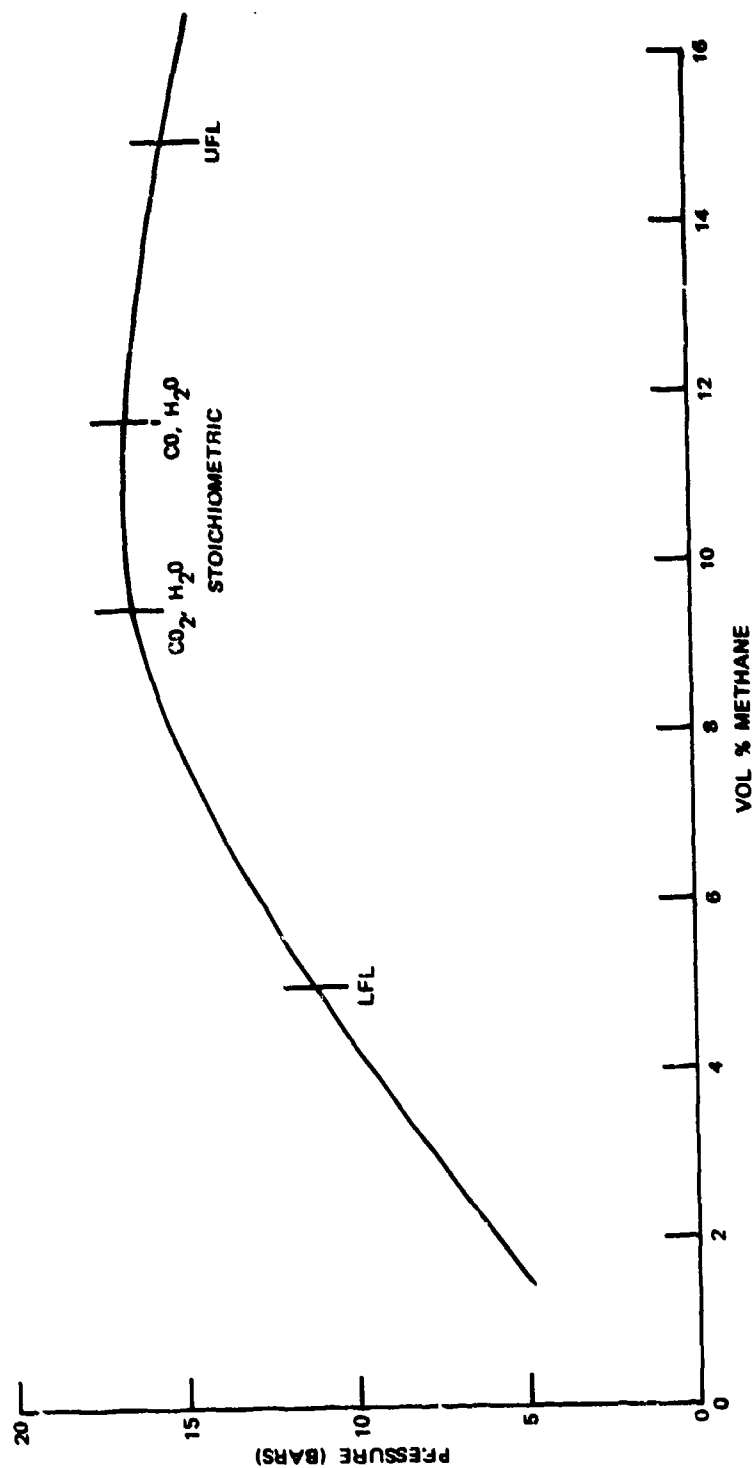


FIGURE 2. Calculated Detonation Pressure, Methane/Air.

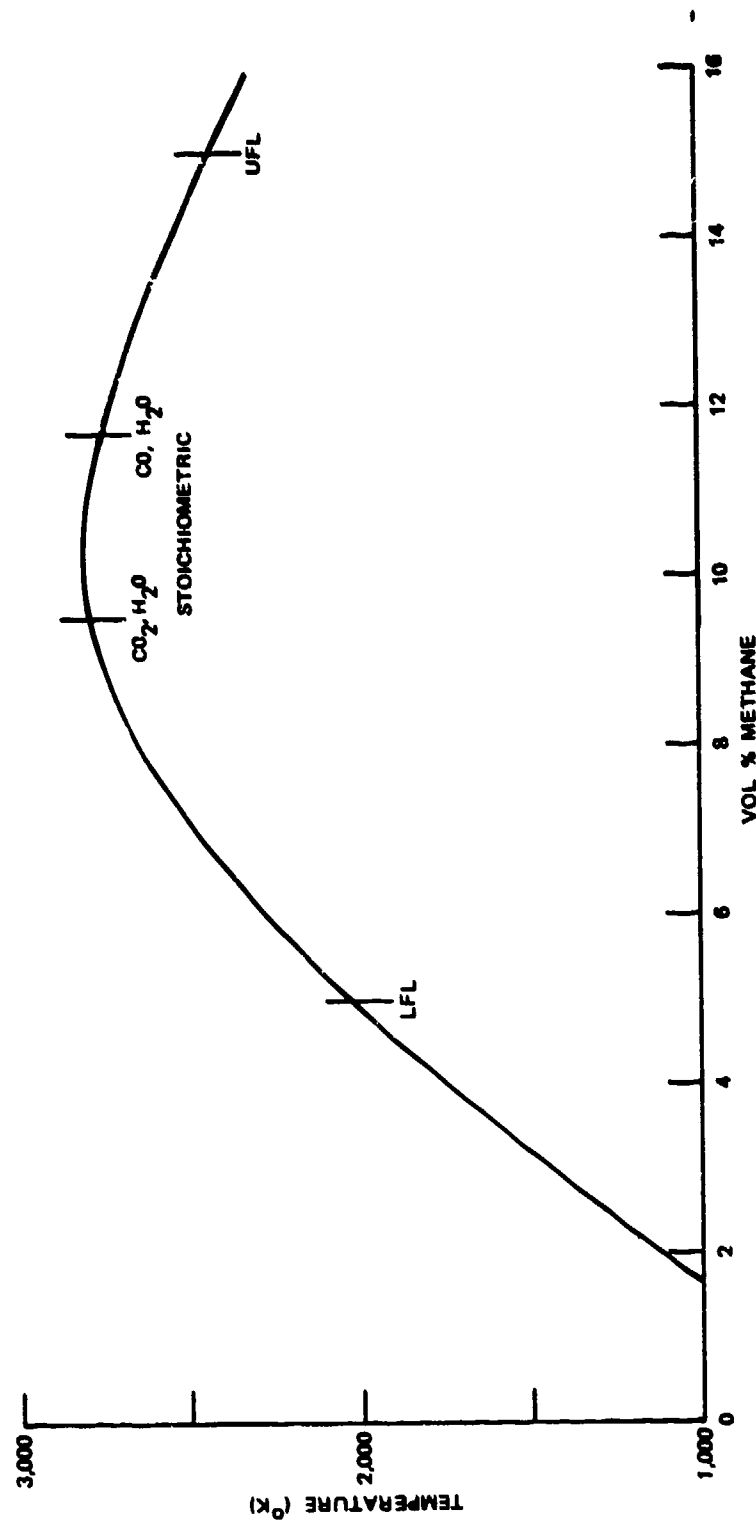


FIGURE 3. Calculated Detonation Temperature, Methane/Air.

theoretically examined three geometries: (1) a spherically expanding wave with no boundaries, (2) a hemispherically expanding wave starting at a free boundary, and (3) a cylindrically expanding wave bounded on one end by a free boundary and on the other by a rigid boundary. The first case is equivalent to a thick cloud initiated at the water surface. The second case is equivalent to a thick cloud initiated at an air/cloud interface. The third corresponds to an initiation of a thin cloud.

The approach was to assume that a flame front expands from the ignition point and a shock wave is formed and propagates ahead of the flame front. A set of equations were then formulated stating: the conservation of mass over the entire reacting zone, the conservation of momentum across the shock zone, and a second conservation of mass over the flame zone. An examination of the conditions which led to a solution of this set of equations yielded a relation between flame and shock strength. The relation was similar for the three geometries treated; however, for a given flame speed the shock strength was highest for the spherical case, next highest for the hemispherical case, and weakest for the cylindrical case.

In order that the non-ideal explosion described by the equations change to an ideal detonation, it is necessary that a flame reaction directly support the shock wave. Two mechanisms for the occurrence of this transition were investigated: (1) a rapidly accelerating flame front, and (2) a thermal explosion of the methane/air mixture behind the shock wave.

The conclusions reached by this study are as follows. A non-ideal explosion could produce a damaging pressure wave over distances from the cloud of the order of magnitude of the cloud height, but for distances greater than roughly ten times this height the shock should be rather weak. In clouds of expected sizes, both flame acceleration and thermal explosion mechanisms of detonation development do not appear likely. It should be pointed out that this is a preliminary study and that more detailed calculations and experimental verification needs to be carried out before the development of a detonation can be considered impossible. Details of the study can be found in Appendix B.

## VAPOR CLOUD EXPLOSION STUDY

An experimental investigation of gas/air explosions must be carried out under conditions which simulate those of an accidental spill. However, the conditions must be sufficiently controlled so that the results can be interpreted. It appears that these are conflicting requirements and no single experiment has been devised to meet both requirements exactly. Therefore, three different experiments are planned: (1) gas/air filled plastic film hemispheres, (2) explosively dispersed liquified gas, and (3) liquified gas spill.

In addition to the above experiments, preliminary tests will be made on each gas mixture in the detonation tube. These tests will determine the adequacy and reliability of the ignition source, the flammability limits (if not known), the detonation

limits (if a detonation can be produced), and the shock strength needed to produce a detonation. The detonation tube will also be used to test some of the instrumentation (photodetectors) used in the larger tests. The detonation tube facility is shown in Figure 4.

The gas/air filled plastic film hemisphere experiment consists of initiating a gas/air mixture in a plastic film hemisphere and measuring the pressure, wave speed and intensity, and the flame front speed.

The theoretical description developed in the first phase of the program indicated that, for a given flame speed, the pressure in the shock wave was higher for the case where no free surface (cloud/air interface) was involved. Thus if a transition to a detonation occurs it will probably happen before the shock wave reaches a cloud boundary. In the case of thin clouds, as are produced by LNG, this distance would be a maximum of the cloud thickness. For a 10,000 m<sup>3</sup> spill this thickness is predicted to be 18 meters. It would be desirable to carry out experiments on this scale; however, as a compromise, 10-meter experiments are planned, and to study the early development of the flame front, 5-meter hemispheres will be used. The hemispherical shape maximizes the shock and flame travel distance before a boundary is reached for a given gas volume and plastic film cost.

Either a spark or a pyrotechnic igniter will be used to ignite the gas/air mixture. In either case an ignition source will be used that will reliably ignite the mixture but which will not produce a shock wave or excessive turbulence. The ignition source will be tested for reliability in the detonation tube before it is used in the hemispherical experiments.

Electronic instrumentation will consist of ten gauge stations in a line flush with the ground. Each gauge station will have one piezoelectric pressure transducer and one photodetector. The output of each pressure transducer will be recorded on a separate channel of an instrumentation tape recorder. The photodetector signals will be electrically mixed and recorded on an eleventh channel. Thus the time of arrival and pressure as a function of time for the pressure wave, and the time of arrival of the flame front will be recorded. Photographic coverage will be by two high speed cameras; one at 4,000 frames/second and one at 400 frames/second. One of the cameras will be mounted over the test pad so that an overhead view can be obtained. In addition, in one of the tests a real time documentation film will be made. Additional photographic coverage can be obtained if initial tests indicate more data could be obtained.

The advantages of this experiment are: (1) gas concentration can be controlled, (2) the geometry of the experiment is known, and (3) the time of initiation is not critical. In addition, the geometry is simple and the results can be used directly to test the theoretical formulation developed in Phase I. The disadvantages of this experiment are that in two respects it does not simulate the accident conditions: (1) there are no concentration inhomogeneities, and (2) the presence of the plastic film. Concentration inhomogeneities, which would be present in a cloud formed by an accidental spill, may affect the flame acceleration although this should have a minor effect. The effect of the film would be to reflect pressure waves back into the flame region. However, if

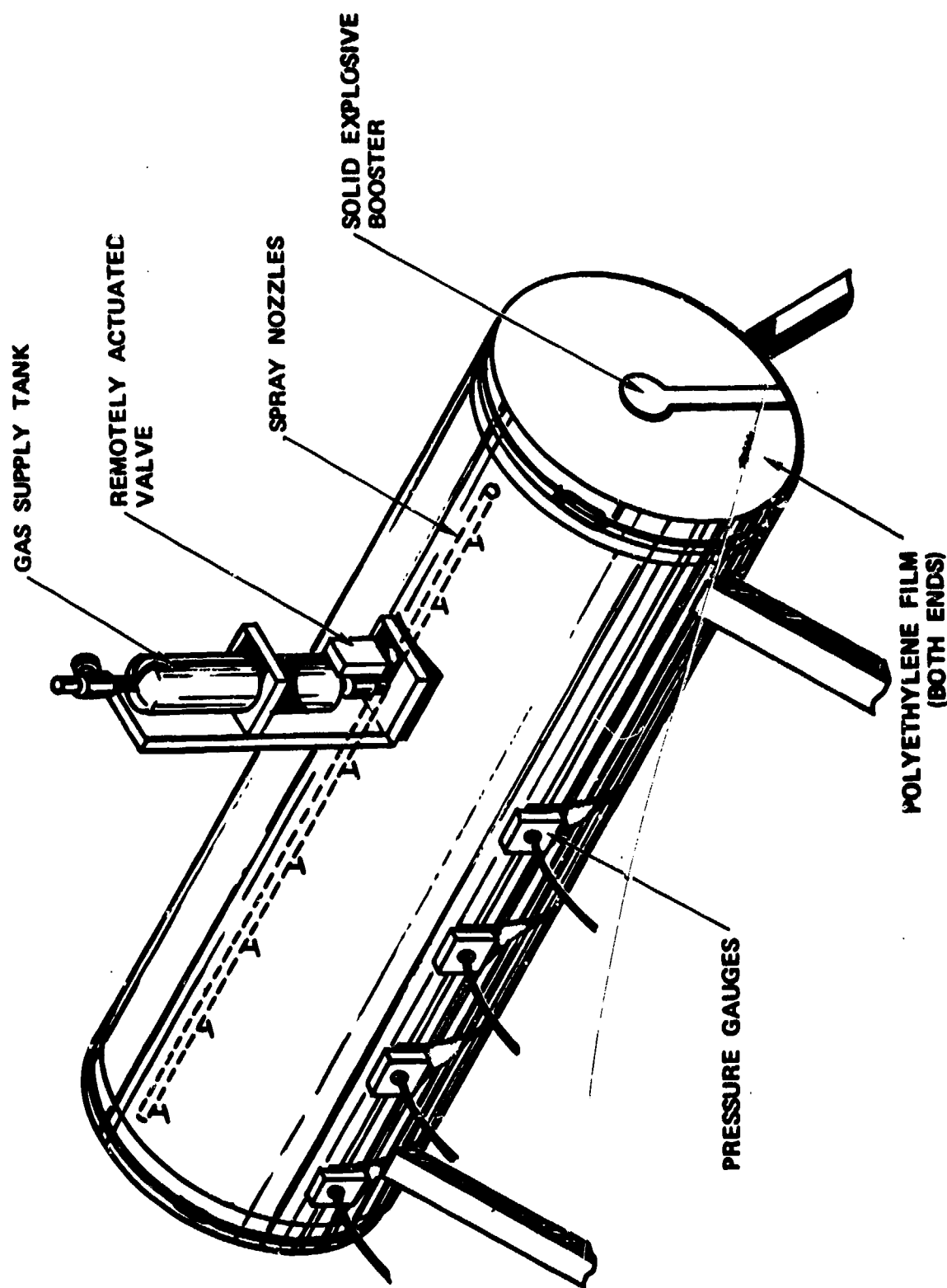


FIGURE 4. Detonation Tube Facility.

the pressure buildup is slow, the film will burst at  $1.4 \times 10^{-3}$  bars, a very low pressure. If the pressure buildup is fast, i.e., a shock wave, there will be a reflection but because of the thinness of the film and the low area density ( $60 \text{ g/m}^2$ ), the reflection will be weak and in the accidental spill case there are bound to be some reflecting surfaces present.

The distance the flame front travels ( $D_F$ ) before it can be disturbed by a reflected shock wave, for the 10 meter radius hemisphere, is

$$D_F = 20F/(V + F)$$

where  $F$  and  $V$  are the flame velocity and shock velocity, respectively. In small spherical experiments, Kogarko measured flame velocity of 10 m/sec which gives a flame travel distance of 0.6 meter (sonic shock velocity). However, this was a small experiment and the flame was accelerating. If the flame has an average velocity of 80 m/sec the travel distance will be 4 meters. Thus an unknown but perhaps significant observation time will pass before any reflection returns from the film. The effect of reflections and turbulence in the flow field will be specifically studied in some of the experiments by deliberately introducing reflecting structures.

If a detonation occurs, as evidenced by pressure records or photographic coverage, the possibility of a detonation in an accident is proven. An examination of the conditions necessary for detonation will then be made to determine if steps can be taken to prevent its accidental occurrence. If no detonation occurs, flame speed/shock wave speed and pressure relationships will be examined to determine if they fit the theoretical model developed in Phase I. If the flame radius/shock radius ratio remains constant, a similarity condition exists and a detonation cannot occur unless the pressure is sufficiently high ( $>10$  bars) to cause a thermal explosion. If, however, the flame radius/shock radius ratio is increasing, a detonation could result when the flame catches the shock. Details of the experimental arrangement for the 5 m radius hemisphere tests are shown in Figures 5 and 6. The 10 m radius tests will have the same general arrangement.

The explosively dispersed liquified gas experiment consists of dispersing liquified gas with a solid explosive burster charge. Then approximately 0.1 second later the formed cloud will be ignited. Time of ignition will be chosen so as to allow the turbulence from the dispersion to abate but before the cloud concentration decreases below the flame limit. The advantages of this experiment are: (1) it is completely free-air (no confinement), (2) concentration inhomogeneities are present (although on an unknown scale), and (3) the geometry is sufficiently known so that pressure gauges can be used and interpreted. The disadvantages are: (1) the concentration is unknown, (2) sequencing the ignition is critical, and (3) considerable hardware development is required to develop a container and dispersion system that will disperse the liquid without ignition. In addition, the geometry is sufficiently complex so that it will be difficult to relate the results with the theoretical model. The reason the geometry is complex is that the explosive dispersion produces a cloud with low fuel concentration at the center so that central ignition cannot be used. In general, the instrumentation and analysis of results will be the same as with the plastic film hemisphere; however, because of the complex geometry more reliance will be placed on the photographic coverage. A 100 kg container is contemplated but the size will depend on the dispersion system developed.



The liquified gas spill experiment will consist of spilling the liquified gas on the pond at area CT-6 and allowing the gas to evaporate and form a cloud. The formed cloud will then be ignited. The advantages of this experiment are: (1) it accurately simulates (except for atmospheric conditions), on a small scale, the accidental spill, and (2) it gives experience in handling a spill for the larger experiments planned for Phase III. The disadvantages are lack of control of (1) the concentration, (2) the geometry, and (3) the time for ignition. Because of the location (over a pond) pressure measuring instrumentation will be difficult to arrange. In addition to determining the combustion behavior of clouds formed by a liquified gas spill on water, the cloud formation and dispersion for ammonia will be studied. This work is an extension of Coast Guard Project CG-22,182A, carried out by A.D. Little, Incorporated. This company would act as a consultant and provide some of the equipment and materials needed for this phase.

Explosive behavior studies of saturated hydrocarbon/air mixtures indicate that all hydrocarbons (other than methane) behave similarly, but that methane is more stable (more difficult to detonate). Therefore, even though LPG has a varying composition it is expected that tests on a given sample will be representative of all LPGs. Natural gas with a high concentration of methane will have to be tested and, in addition, the fraction of higher hydrocarbons added to natural gas which affect its properties needs to be determined.

The specific tests to be carried out are as follows:

1. Detonation Tube Tests. Preliminary tests will be carried out in the detonation tube on natural gas, LPG, ammonia, ethylene, butadiene, and vinyl chloride. Facilities are available to test other gases at the sponsor's request
2. Small Hemisphere Tests (5 meter radius). A study of the early development of the flame front will be carried out in 5-meter radius film hemispheres. Three experiments with LPG, three with natural gas, and two with mixtures of natural gas and LPG are planned.
3. Large Hemisphere Tests (10 meter radius). Based on the results of the small hemisphere tests, a total of four tests will be carried out in the 10-meter radius film hemispheres. A total of twenty film hemispheres (10 x 5 meter radius and 10 x 10 meter radius) will be purchased so materials will be available for future tests.
4. Liquified Gas Spill. The A. D. Little work will be extended to 1,500-gallon spills of liquid anhydrous ammonia. This will involve purchase and installation of a 1,600-gallon capacity cryogenic liquid gas tank and delivery of the system at the CT-6 test site, and installation of gas monitoring instrumentation downwind of the spill point. Four 1,500-gallon spills are planned with materials available for a fifth test if required. The facility is planned so that it can be used for future explosive tests with LNG or other materials.

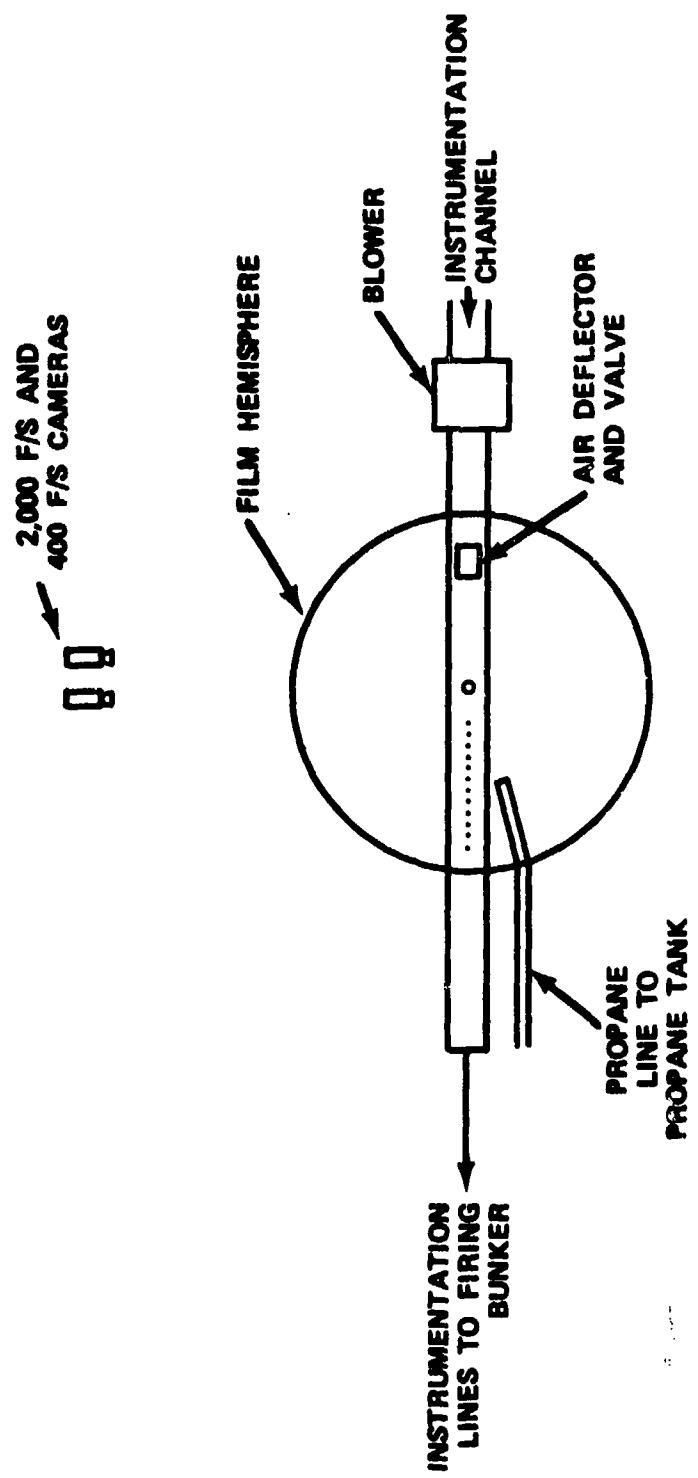


FIGURE 5. Hemisphere Test, 5m Radius (overhead view).

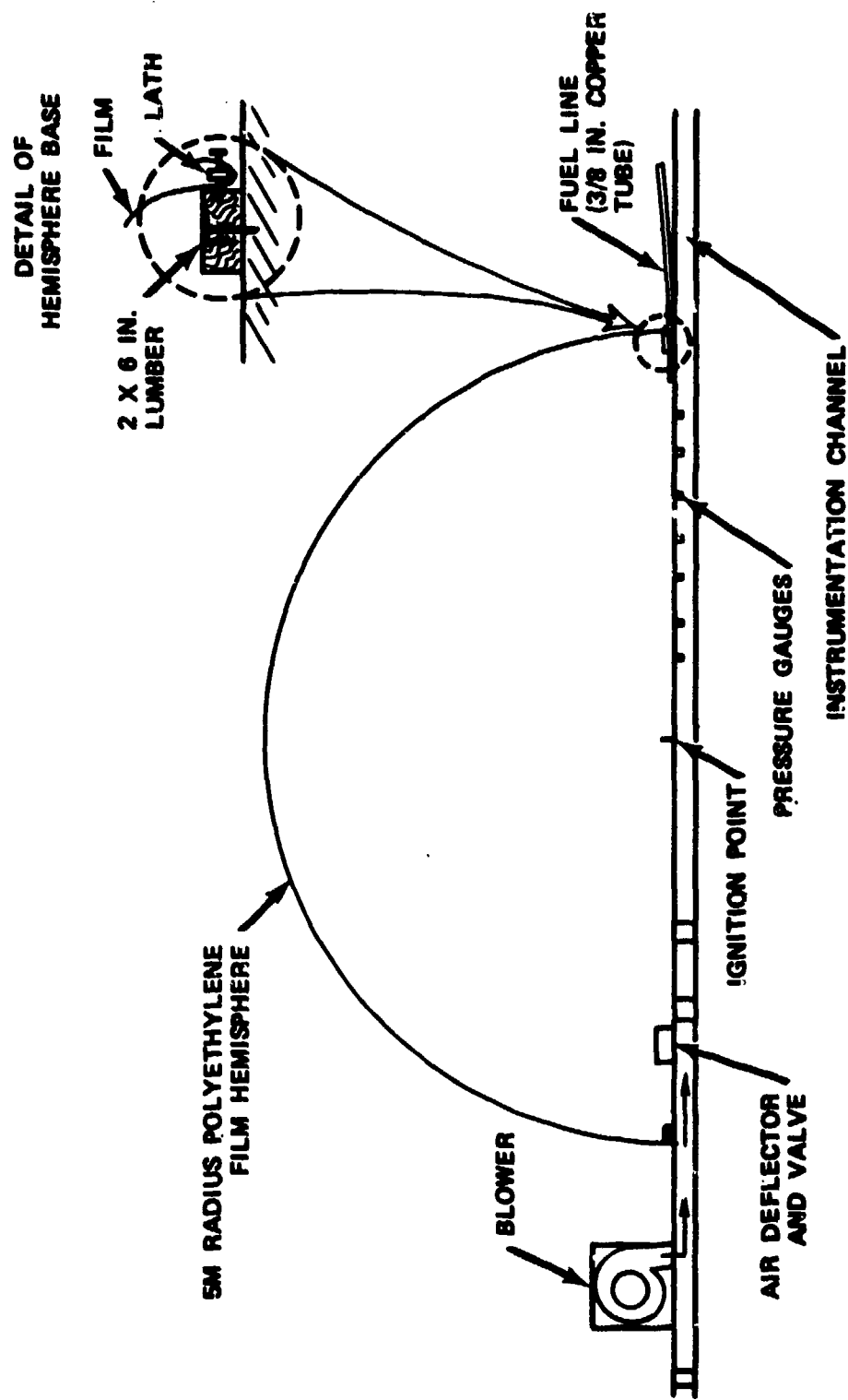


FIGURE 6. Hemisphere Test, 5m Radius

5. Explosive Dispersion. A preliminary engineering design study will be made of the hardware necessary for the explosive dispersion experiments. This will include design of explosive dispersion cannisters in two different sizes, 40 and 150 kg.

Subsequent to the writing of this report, three 5 m radius hemispherical tests were carried out. Two of the tests were with 4% by volume propane in air and the third was with 5% by volume propane. In none of these tests did a detonation occur. The flame front velocity was 6.30 m/sec for the 4% propane and 7.37 m/sec for the 5% propane. The flame front velocity appeared constant in both cases.

## APPENDIX A

### CALCULATION OF METHANE VAPOR CLOUD GENERATION AND DISPERSION

#### INTRODUCTION

The method of calculation is based on the report, *Spills of LNG on Water*, Esso Research and Engineering Company, Report EE61E-72. The main purpose of the Esso work was to calculate and experimentally verify the total area on the water that would at any time have a concentration of methane vapor of at least the lower flammability limit (5%). Since the experimental work indicated local turbulence produced a peak to average concentration ratio of 2, the calculations actually were for the area covered by a concentration of at least 2.5%. The calculation of higher concentration as a function of space and time required some modification of the calculations and should be considered an approximation until experimental verification or a more rigorous mathematical model can be developed.

#### CALCULATION PROCEDURE

##### Step 1 - Definition of Input Conditions

Calculations were made for three spill sizes; 4,000, 10,000, and 50,000 m<sup>3</sup>. Other than spill size, the conditions were the same for all three calculations, i.e., wind speed - 2.24 m/sec, horizontal dispersion coefficient - Pasquil C, vertical dispersion coefficient - Singer and Smith D, air temperature - 21°C, relative humidity - 75%.

##### Step 2 - Calculate Liquid Pool and Vaporization Parameters

$\theta_{\max}$  is the time, measured from the instant of spill, at which the pool has reached maximum diameter ( $D_{\max}$ ), minimum thickness ( $t_{\min}$ ), and maximum boil off ( $w_{\max}$ ). These quantities are calculated as follows. At any time  $\theta$  the total weight spilled is divided between material that remains on the water surface and that which has boiled off.

$$w^* = \rho V = (\pi/4) D^2 t \rho + \int_0^\theta (\pi/4) D^2 R d\theta \quad (1)$$

Combining Eq. (1) with the experimentally determined relations given in the Esso report:

$$D = 1.27 \theta \quad (2)$$

$$t = 1.01 \times 10^{-3} D^{0.56} = 1.15 \times 10^{-3} \theta^{0.56} \quad (3)$$

yields

$$w = 0.664 \theta^{2.56} + 0.0845 \theta^3$$

This can be solved for total weight spilled to give  $\theta_{max}$  and this value used in Eq. (2) and (3) to give  $D_{max}$  and  $t_{min}$ . The Esso report evaporation rate of  $0.196 \text{ kg/m}^2/\text{sec}$  yields a boil-off rate of:

$$\dot{w} = \pi/4 D^2 R = 0.25 \theta^2, \quad (4)$$

and the max value  $\dot{w}_{max} = 0.25 \theta_{max}^2$ . (5)

### Step 3 - Calculate Vapor Accumulation and Vapor Flow Rate

A graphical method is used to calculate vapor accumulation over the pool and the downwind vapor flow rate. First, the boil-off rate ( $\dot{w}$ ) given by Eq. (4) is plotted versus time from 0 to  $\theta_{max}$ . This is the boil-off rate as the pool expands. The pool thickness is then assumed to remain constant and, as material evaporates, the pool decreases in diameter and the boil-off rate decreases and is given by:

$$\dot{w} = \dot{w}_{max} e^{[-R/\rho t_{min} (\theta - \theta_{max})]} \quad (6)$$

This rate is plotted from  $\theta_{max}$  until a time is reached when the boil-off is small. It has been found experimentally that the downwind vapor flow rate ( $q$ ) is smaller than the evaporation rate ( $\dot{w}$ ). The ratio  $q/\dot{w}$  is independent of spill size and is a function of wind speed ( $s$ ). The Esso report gives a graphical relation of  $q/\dot{w}$  versus  $s$  which fits the curve:

$$q/\dot{w} = 1 - e^{-0.1s}. \quad (7)$$

From Eq. (7) and the value of  $\dot{w}_{max}$  determined by Eq. (5), the value of  $q_{max}$  may be calculated. The time at which the maximum vapor flow rate occurs ( $\theta_q$ ) is not the time of maximum boil-off ( $\theta_{max}$ ) but at some time later when the boil-off rate drops to the vapor flow rate, i.e.,  $q_{max} = \dot{w}$  or

$$q_{max} = \dot{w}_{max} e^{[-R/\rho t_{min} (\theta_q - \theta_{max})]} \quad (8)$$

This equation can be solved for  $\theta_q$ :

$$\theta_q = \theta_{max} - (\rho t_{min}/R) \ln (q_{max}/\dot{w}_{max}). \quad (9)$$

Had the spill been smaller, the pool spread would follow the same curve but would terminate sooner at some smaller value of  $\dot{w}_{max}$ ;  $\dot{w}$  would decay and would intersect the  $q$  curve sooner at a smaller value of  $q_{max}$ . Thus, the  $q$  curve is really the locus of  $q_{max}$  values corresponding to each value of  $\dot{w}_{max}$  and the  $q$  versus  $\theta$  curve can be calculated in the same manner that  $\theta_q$  and  $\theta_{max}$  were calculated. The curves calculated ( $\dot{w}$  and  $q$  versus  $\theta$ ) for the  $10,000 \text{ m}^3$  spill are shown in Figure A-1. The area between the  $\dot{w}$  curve and the  $q$  curve is the vapor accumulation ( $w_{acc}$ ) over the spill site. If the cloud of accumulated vapor is assumed cylindrical with a diameter equal to the maximum pool diameter, the height is then:

$$h = w_{acc}/\rho (\pi/4) D_{max}^2. \quad (10)$$

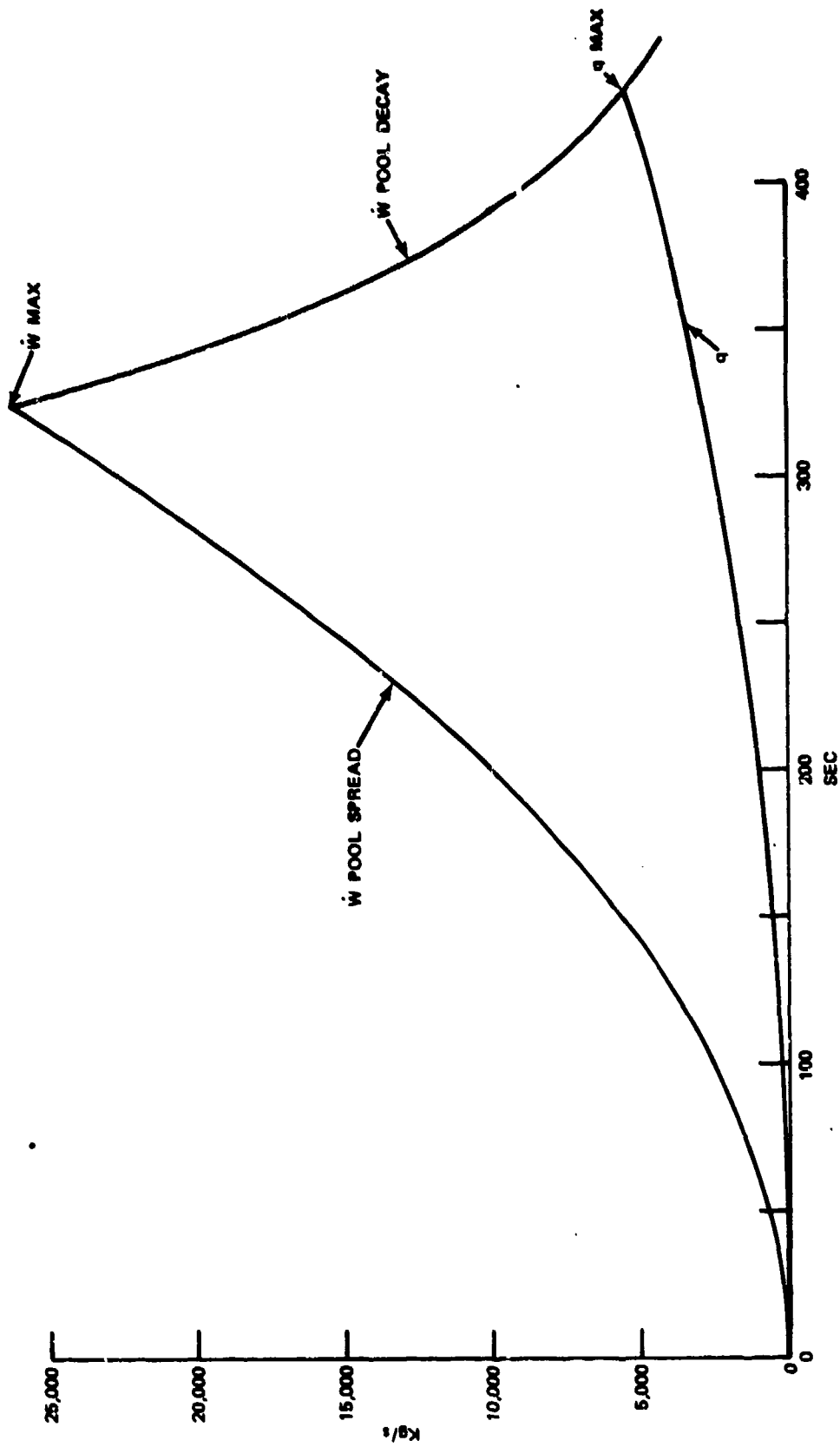


FIGURE A-1. Vapor Accumulation, 10,000 m<sup>3</sup> Spill.



This ends the calculation of spill point conditions.

#### Step 4 - Calculation of Vapor Cloud Gravity Spread

Air at 21°C and 75% relative humidity has a density of 1.19 kg/m<sup>3</sup>. The methane vapor as it forms over the pool has a density of 1.84 kg/m<sup>3</sup>. The vapor will spread due to gravity as it moves downwind until it warms and mixes with air and its density equals air density. The warming is not only due to mixing with air, but also to heat transfer from the water. The combined effects are given in the Esso report in tabular form as values of percent by volume methane (C) and vapor/air mixture ( $\rho$ ). The data fits the curve:

$$\rho = 1.175 - 1.08 \times 10^{-3} C + 6.86 \times 10^{-5} C^2 \quad (11)$$

Solving Eq. (11) for the concentration of methane (C) that gives a mixture density equal to the air density yields a limiting concentration of 24%.

The plume achieves velocity by momentum transfer from the air which dilutes it. A momentum balance yields a linear relation between methane weight percent and fraction of wind speed attained. Combining this relationship with the definition of weight and volume percent (C) yields Eq. (12) where u is the plume velocity.

$$u/s = 1 - ((1.23C)/(223 - C)) \quad (12)$$

Cloud height was calculated by Eq. (10). The value was obtained by assuming that the entire difference between q and w was due to accumulation and that wind drift and diffusion are negligible. In the Esso report experimental values of 60% of the calculated height were reported. This factor of 0.6 was used in their calculations and will be used here. It should be pointed out that this is an arbitrary value and this is one area where the math model could be improved.

In the gravity spread calculation it is assumed that the vapor flow rate is constant at the maximum rate ( $q_{max}$ ) given by Eq. (7). At any downwind point a material balance across the plume shows that:

$$\text{Plume mass flow rate} = 100 \text{ q/wt \%} = \rho h L u \quad (13)$$

Solving for plume width (L) and replacing wt % by an expression involving volume % gives:

$$L = [(223 - C) q] / (1.23 C h u \rho) \quad (14)$$

The plume lateral spread rate is given by the equation of Fannelop and Waldman:

$$(dL)/(dx) = 1.47 [(\Delta\rho/\rho) (g h L)/(x u^2)]^{1/3} \quad (15)$$

On integration between the limits L to L<sub>0</sub> and 0 to x, Eq. (15) becomes:

$$x^{2/3} = 0.681 \left[ (L^{2/3} - L_0^{2/3}) / (\Delta\rho/\rho \cdot (g h)^{1/2}) \right]^{1/3}. \quad (16)$$

Using Eq. (14) to determine plume width (L) and Eq. (16) to calculate the downwind distance (x) in a stepwise fashion, a table of L and x is constructed for decreasing values of concentration (C) from 100% to the limiting value where the plume density equals air density. In addition, from the plume velocity (u) and the downwind distance (x), the time to reach various downwind distances can be calculated. This ends the gravity spread part of the calculations.

#### Step 5 -- Calculation of Atmospheric Dispersion

The Pasquill equation is used to calculate concentration when the mixing is caused by atmospheric mixing:

$$C = \left[ (151 q) / (\pi u \sigma_y \sigma_z) \right] e^{-[y^2/2\sigma_y^2 + z^2/2\sigma_z^2]}, \quad (17)$$

where  $\sigma_y$  and  $\sigma_z$  are empirically determined atmosphere dispersion coefficients. To facilitate calculation on a programmable desk computer the Esso curves have been expressed as functions of downwind distance (x):

$$\sigma_y = 0.17 x^{0.92}, \quad (18)$$

$$\sigma_z = 0.0703 x^{0.694}. \quad (19)$$

Since the vapor plume at the end of the gravity spread phase is not a point source at sea level, two modifications to the Pasquill equation must be made. The first is to add to the vertical dispersion coefficient a correction to correct for plume height. This correction is the height converted to a standard deviation.

$$\sigma_z = 0.0703 x^{0.694} + (h/1.25). \quad (20)$$

The second is to divide the vapor flow into multiple sources in a line in the y direction. The total concentration is then found by summing the concentration from each individual source. With these modifications and considering first the sea level concentration, the Pasquill equation becomes:

$$C = \sum_n \left[ (151 q/n) / (\pi \sigma_y \sigma_z u) \right] e^{-y^2/2\sigma_y^2}. \quad (21)$$

where  $\sigma_y$  is given by Eq. (18) and  $\sigma_z$  by Eq. (20).

By means of Eq. (21), cross wind sea level concentration profiles are calculated as a function of downwind distance (x). The vertical concentration is then calculated as follows:

$$C = C_{SL} e^{-z^2/2\sigma_z^2} \quad (22)$$

where  $C_{SL}$  is the sea level concentration.

### Step 7 - Calculate the time Variation of Plume Shape

During the pool spread phase it was assumed that a vapor accumulation took place above the pool. The gravity spread and atmospheric dispersion were then calculated assuming that vapor flowed from this accumulation at a constant rate, in other words, a steady state process. The plume width and height during the gravity spread phase and the concentration profiles calculated during the atmospheric dispersion phase at any downwind distance ( $x_1$ ) are thus time invariant from the time the plume reaches the point  $x_1$  until the accumulation is exhausted and the back of the plume reaches point  $x_1$ . The front of the plume moves with the velocities calculated and arrives at downwind distances in the times calculated during the gravity spread phase. During the atmospheric dispersion phase it is assumed the plume front moves at the wind speed ( $u$ ) and the time to reach any given distance can be calculated from this velocity.

The time when the vapor accumulation is exhausted will be given by:

$$\theta = (\rho_1 V)/q . \quad (23)$$

Thereafter, the back of the plume is assumed to move with the wind speed and the time for the back of the plume to reach any given downwind distance can be calculated from this velocity.

### RESULTS OF THE CALCULATIONS FOR 4,000, 10,000 and 50,000 m<sup>3</sup> SPILLS

Table A-1 lists the calculated values for 4,000, 10,000, and 50,000 m<sup>3</sup> spills. Figures A-2 through A-6 show calculated concentration profiles for the two spill sizes, and Figure A-7 shows the plume shape at different times after spill for 10,000 m<sup>3</sup> spill.

## LIST OF SYMBOLS USED

$\theta$	time (sec)
D	pool diameter (m)
t	pool thickness (m)
w	weight methane (kg)
$\dot{w}$	boil-off (kg/sec)
$\rho$	density (kg/m <sup>3</sup> )
V	volume (m <sup>3</sup> )
R	evaporation rate (kg/m <sup>3</sup> /sec)
q	vapor flow rate (kg/sec)
h	plume height (m)
C	methane concentration (% volume)
u	plume velocity (m/sec)
L	plume width (m)
x	downwind distance (m)
g	gravitational constant (9.8 m/sec <sup>2</sup> )
y	crosswind distance (m)
z	vertical distance (m)
$\sigma_y$	crosswind dispersion coefficient (m)
$\sigma_z$	vertical dispersion coefficient (m)
$\frac{\Delta \rho}{\rho}$	plume density, air density difference (kg/m <sup>3</sup> ) divided by plume density
$\theta_q$	time of maximum vapor flow rate
$\lambda$	wind speed

TABLE A-1. Results of Calculations.

	1,000 m <sup>3</sup> spill	10,000 m <sup>3</sup> spill	50,000 m <sup>3</sup> spill
Time <sup>a</sup> to maximum pool spread, $\theta_{\max}$ (sec)	233	324	567
Maximum diameter of pool, $D_{\max}$ (m)	297	411	720
Minimum pool thickness, $t_{\min}$ (m)	0.0244	0.0294	0.0401
Maximum boil-off, $\dot{w}_{\max}$ (kg/sec)	13,500	26,244	$8.04 \times 10^4$
Maximum vapor flow rate, $q_{\max}$ (kg/sec)	2,776	5,380	16,130
Time of maximum vapor flow rate (sec)	324	432	717
Vapor accumulation over pool (kg)	$1.39 \times 10^6$	$3.56 \times 10^6$	$1.74 \times 10^7$
Actual height of accumulation (m)	10.9	14.6	23.2
Assumed height of accumulation (m)	6.55	8.75	13.9
Plume width at end of gravity spread phase, $L_{\max}$ (m)	1,356	1,967	3,703
Distance downwind at end of gravity spread phase, $x_{\max}$ (m)	404	511	744
Time to reach end of gravity spread phase (sec)	569	745	1,188
Time to exhaustion of vapor accumulation (sec)	733	1,400	1,796
Time for front of plume to reach 1,500 m downwind (sec)	1,058	1,191	1,525

<sup>a</sup>Time zero is instant of spill.

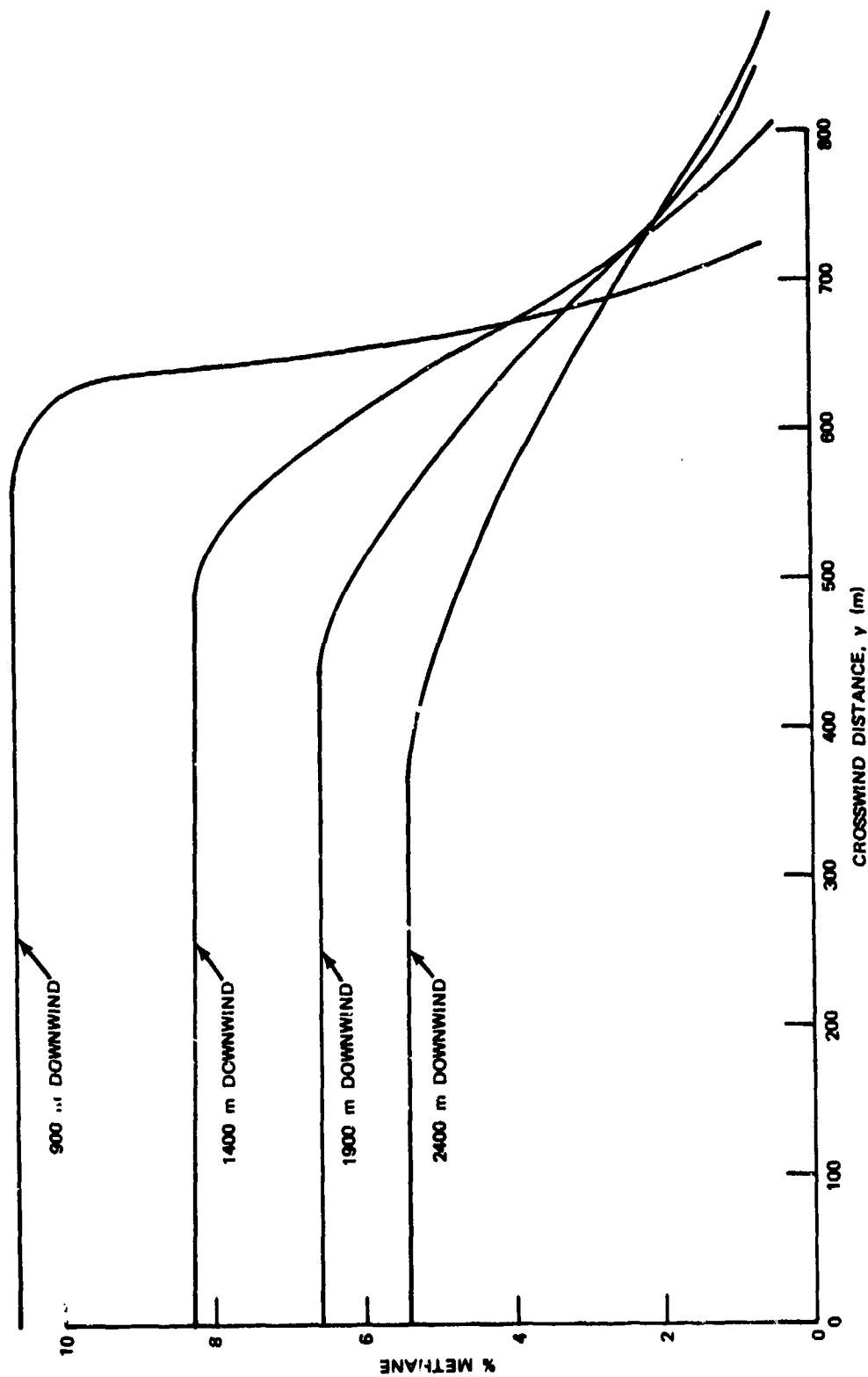


FIGURE A-2. Sea Level Concentration Profile, 4,000 m<sup>3</sup> Spill.

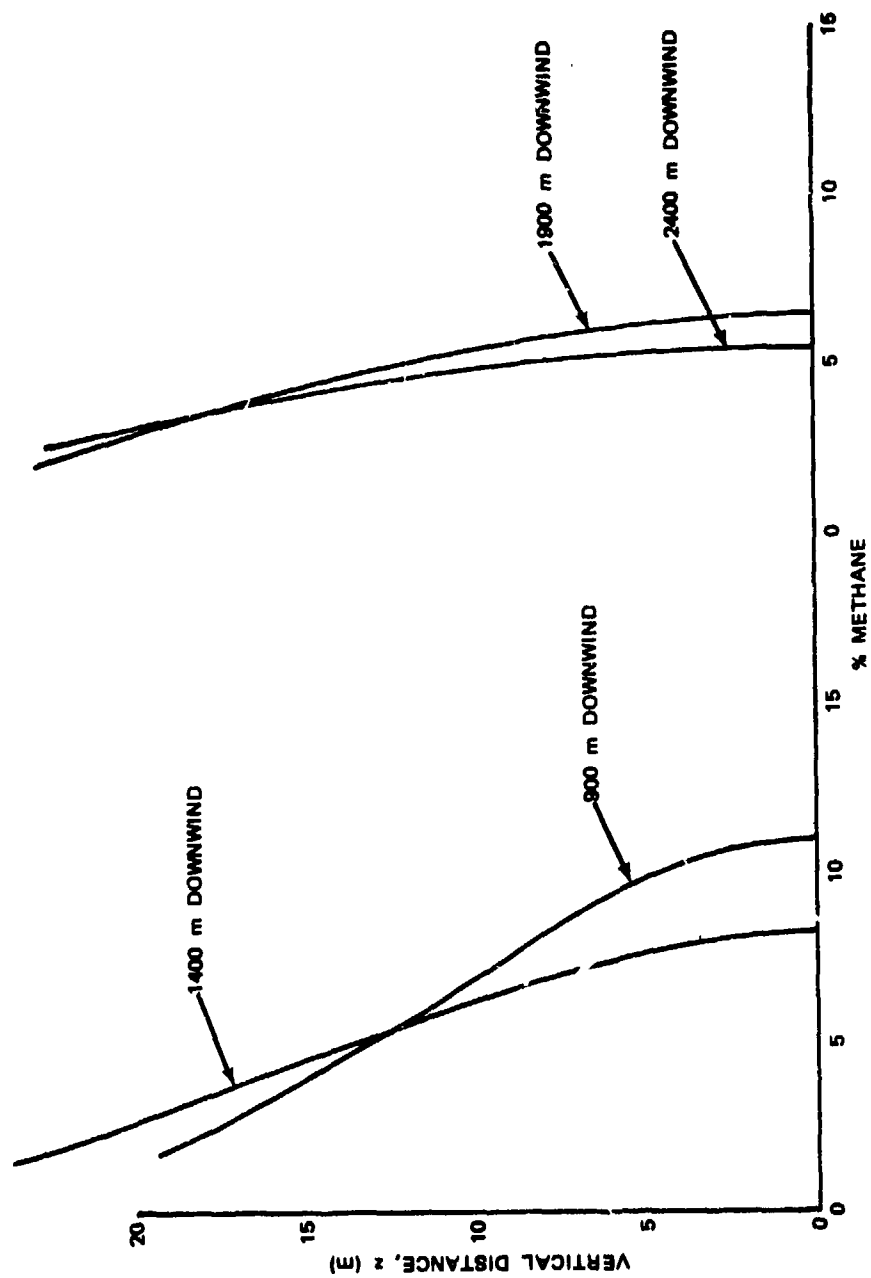


FIGURE A-3. Vertical Concentration Profile, 4,000 m<sup>3</sup> Spill.

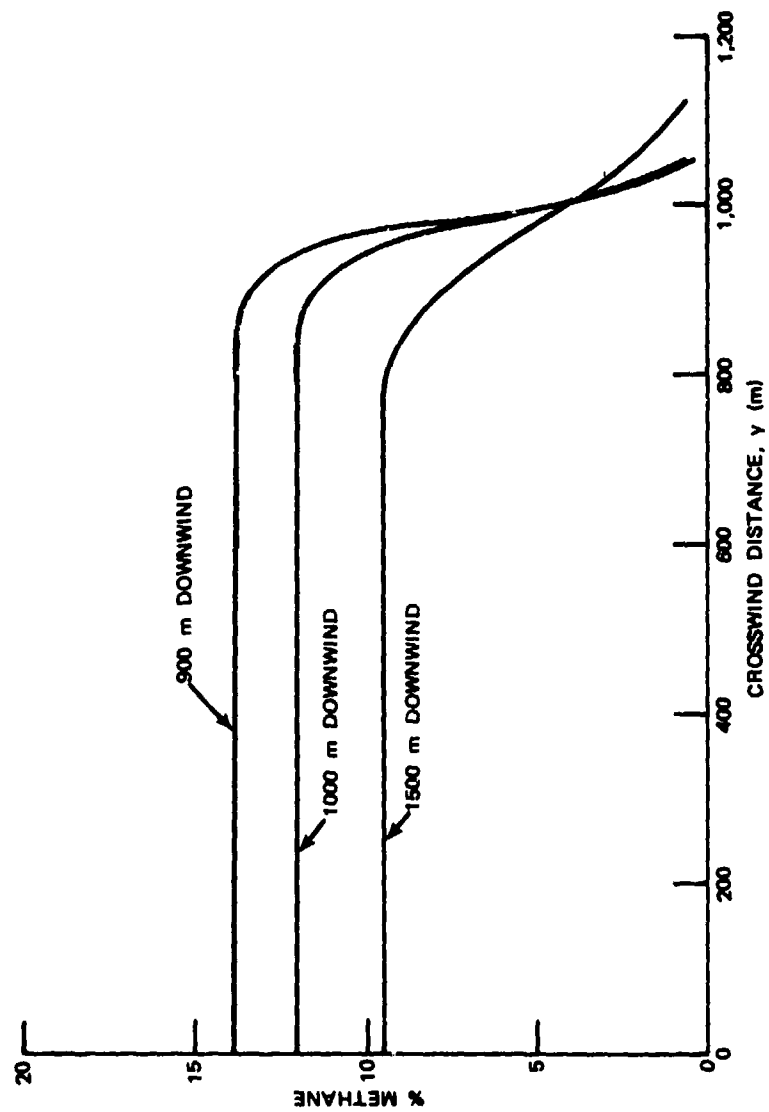


FIGURE A-4. Sea Level Concentration Profile, 10,000 m<sup>3</sup> Spill.



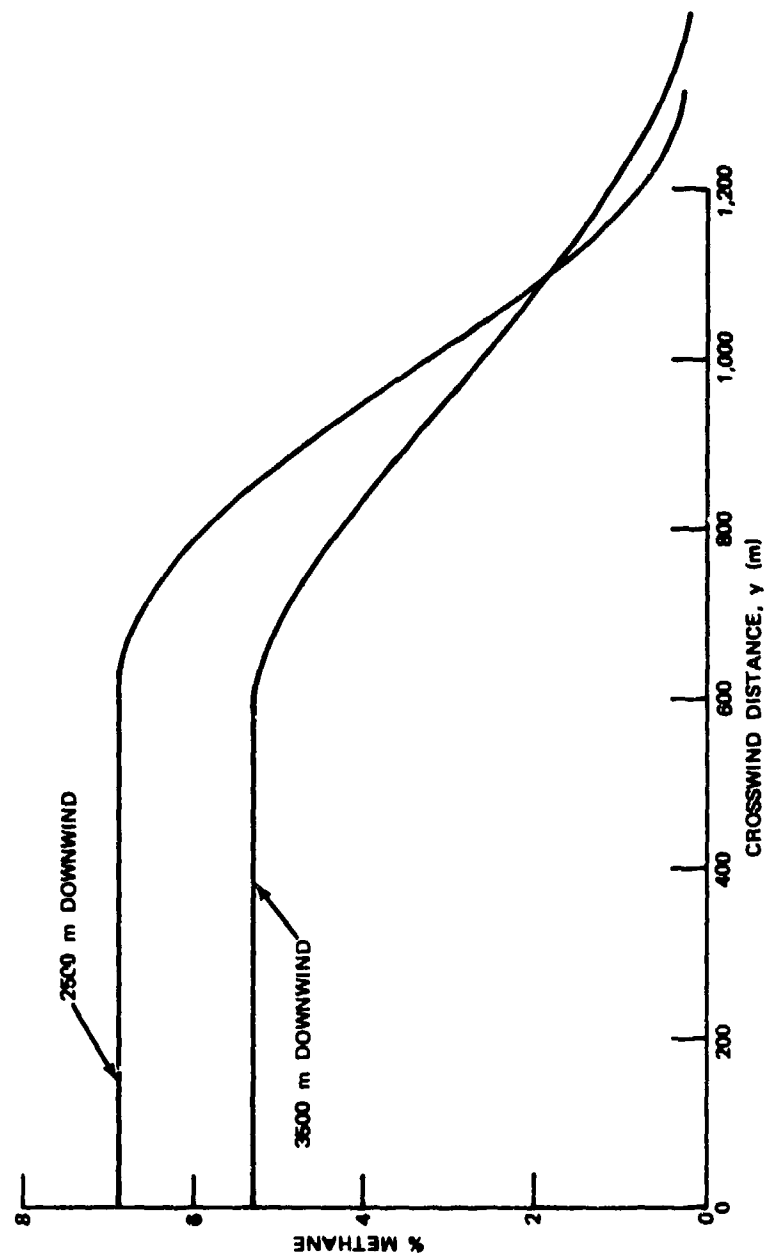


FIGURE A-5. Sea Level Concentration Profile, 10,000 m<sup>3</sup> Spill.

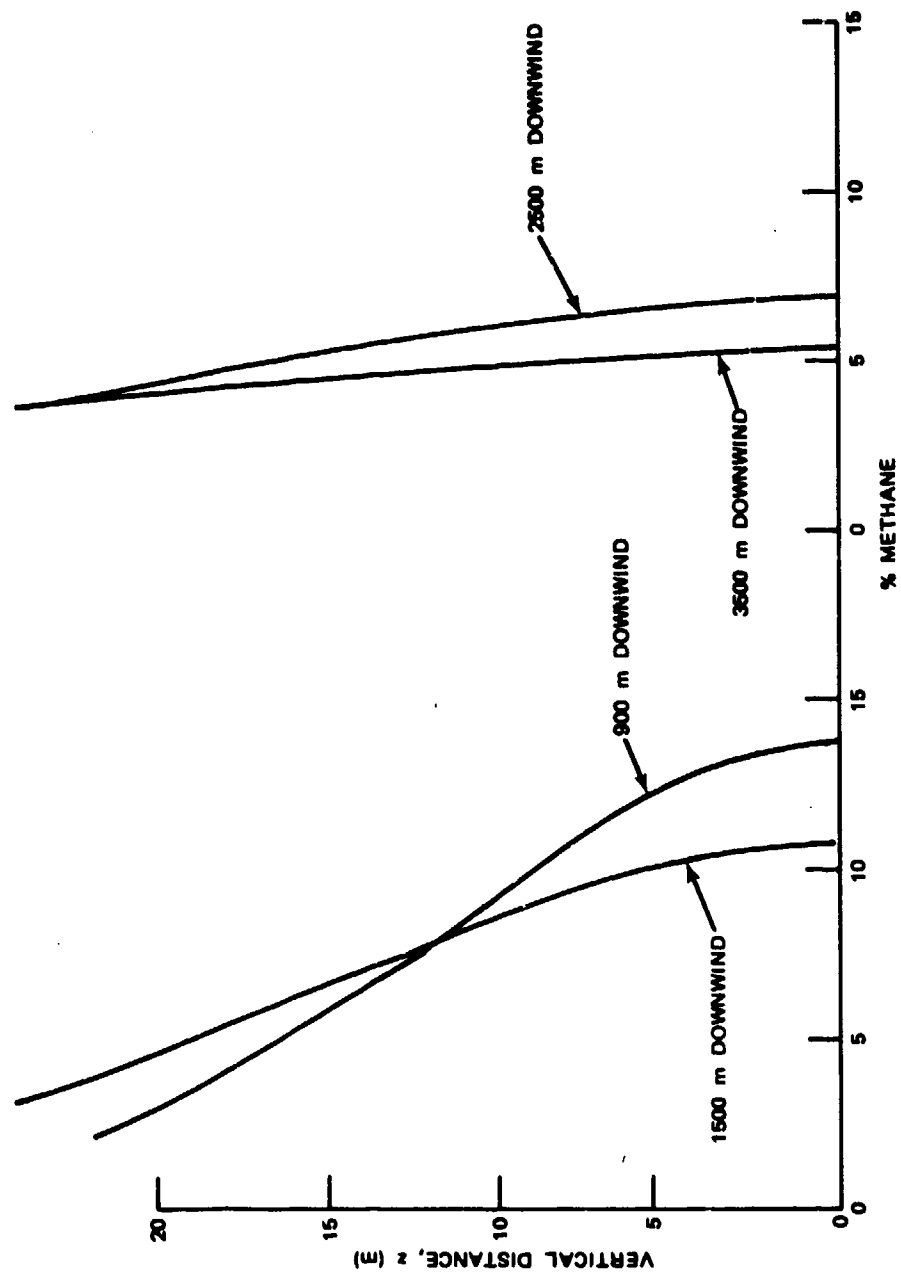


FIGURE A-6. Vertical Concentration Profile, 10,000 m<sup>3</sup> Spill.

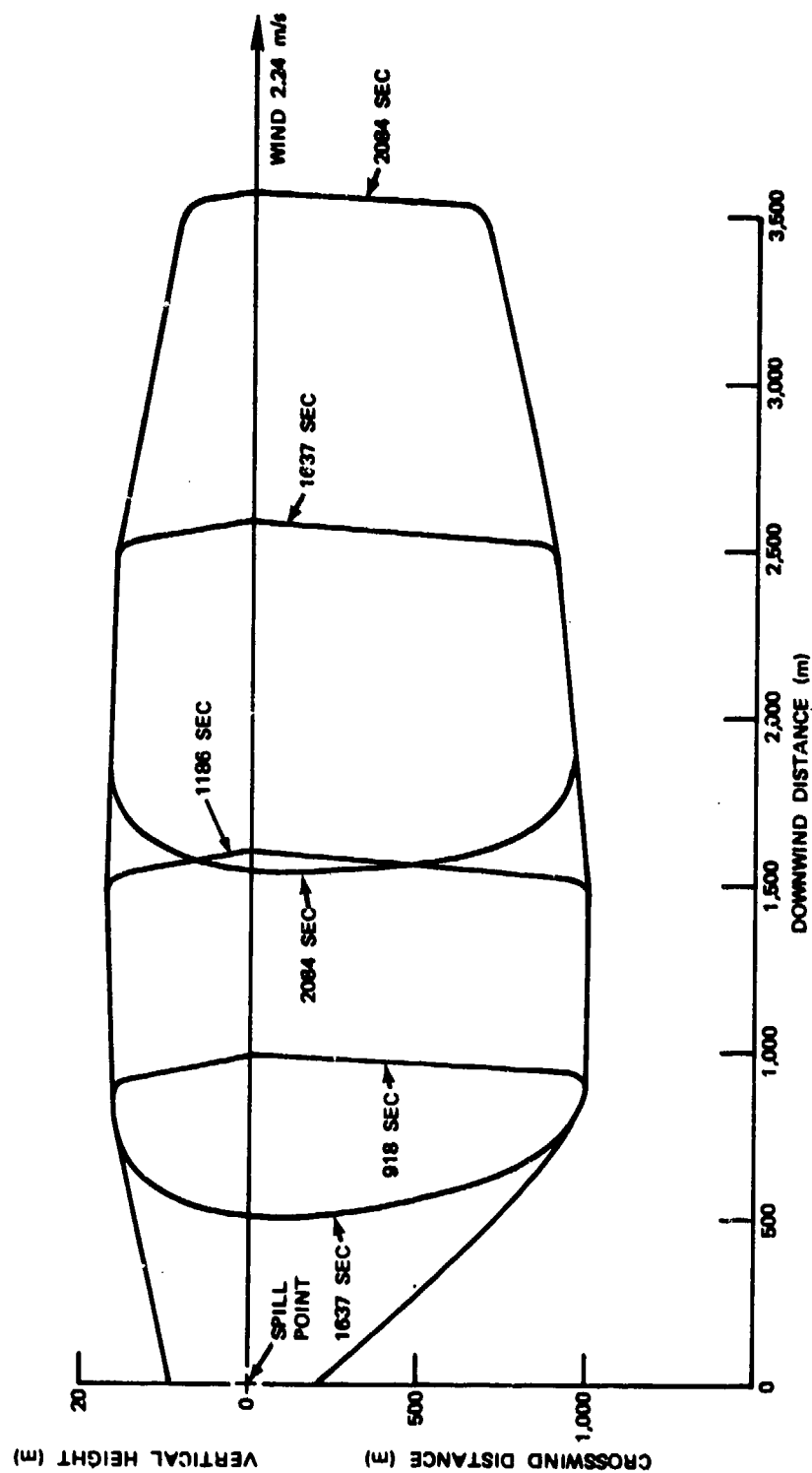


FIGURE A-7. Vapor Plume Shape, 10,000 m<sup>3</sup> Spill, Concentration > 5%.

## APPENDIX B

### QUALITATIVE THEORY OF NON-IDEAL EXPLOSIONS

by

F. A. Williams  
Department of Aerospace and Mechanical Engineering Sciences  
University of California, San Diego

#### INTRODUCTION

In view of the great concern over explosion hazards associated with large LNG spills on water, it is of interest to attempt to develop an understanding of the types of explosions that may occur. It is also desirable to have formulas which may be used to obtain estimates of initial conditions (e.g., critical spill size) needed for a detonation to develop. The considerations outlined herein address these objectives. The intention is to consider a variety of configurations from a common, simplified viewpoint. In this respect, accuracy is sacrificed for generality, and the results must be termed "qualitative".

#### WAVE DYNAMICS OF NON-IDEAL EXPLOSIONS

Given a large LNG spill and its associated vapor cloud, it is most logical to presume that the initiation of any exothermic reaction would occur from a small spark or flame. This type of initiation produces a deflagration rather than a detonation. Since the time required for a deflagration to develop is quite short (at any position where the mixture lies between the flammability limits), the most interesting problem to consider is one in which a flame is propagating through a premixed cloud. The velocity of flame propagation will be denoted by  $S$  and will be treated here as a prescribed quantity. This is reasonable, since flame speeds are functions of temperature, pressure, composition, and turbulence of the mixture into which the flame propagates. Here "turbulence" signifies nonhomogeneities in both velocity and composition; it being recognized that although turbulence often produces flame acceleration, there are many situations in which well-defined turbulent flame speeds exist.

It is well known that a point-initiated propagating flame generates pressure waves, as a consequence of the density decrease across the propagating flame. As acoustic waves are emitted, later ones travel faster than earlier ones, due to the slight increase in sound speed (temperature) across the pressure wave. The result is that the pressure waves emitted by the flame coalesce somewhere to form a shock wave. Analysis of the coalescence process is complicated, and the time and position at which the shock is formed is difficult to calculate. However, it is known that coalescence occurs reasonably rapidly. Therefore, as a starting condition for making an analysis, it seems reasonable to hypothesize, as a simplifying assumption, that a weak shock wave exists at some distance from the deflagration. The shock propagates ahead of the flame with a time-dependent velocity ( $V$ ) which is determined from local and overall conservation conditions.

With specified initial locations of the flame and the shock, the wave pattern will evolve in such a way that the flame continues to emit sound waves which overtake, coalesce with, and usually strengthen the shock. This means that the pressure field is nonuniform in the region enclosed by the shock. The extent of this nonuniformity may be estimated from an accurate calculation for a particular case (Kuhl, A. L., Kamel, M. M., and Oppenheim, A. K., *Pressure Waves Generated by Steady Flames*, Fourteenth Symposium (International) on Combustion, The Combustion Institute, Pittsburgh, 1973, pp. 1201-1215). It is found that the pressure difference between the flame and the shock is comparable with the pressure rise across the shock. Nevertheless, as a primary simplifying assumption, the pressure within the region subtended by the shock will be taken as constant herein. Thus, the field is divided into two parts, the exterior of the shock, at atmospheric pressure ( $p_0$ ) and the interior of the shock at the spatially-independent but time-varying pressure ( $p_1$ ). This simplification is introduced for the purpose of developing readily interpretable results. Since it is unlikely that pressure variations between the shock and the flame would become large compared with the pressure rise across the shock, this simplification is expected to produce results having the correct order of magnitude.

If truly simple results are to be obtained from an analysis, then further simplifications are required. To this end, one must consider the two parts of the field contained within the shock, viz., the region (subscript 2) enclosed by the flame and the region (subscript 1) between the shock and the flame. The principal effect of the flame on the material that it consumes is to heat this material to a very high temperature, giving it a very low density. This density change across the flame probably is larger than the density variations from point to point elsewhere in the material contained within the shock. Therefore, density will be assigned two separate spatially independent (but possible time-dependent) values ( $\rho_1$  and  $\rho_2$ ) in regions 1 and 2, respectively. It should be emphasized that the severity of this approximation probably is comparable with that of the approximation of constant pressure. Since the shock processes different fluid elements at different speeds, and since by the constant-pressure assumption different fluid elements will be compressed adiabatically to different extents before burning, temperature and density variations definitely will exist in region 1.

If  $\rho_1$  is obtained from  $\rho_0$  by use of shock relations, then  $\rho_1/\rho_0 \approx 1.5$  to 6 is reasonable, depending on the strength of the shock. Since the density ratio across a shock varies less than either the pressure ratio or the temperature ratio, the relationship  $\rho_1 = \rho_0/k$ , with  $k$  a time-independent constant whose value is approximately  $k = 1/2$ , could be a useful first rough approximation. Similarly, in view of disassociation of reaction products, the approximation of a constant temperature behind the flame may be better than, for example, the more conventional approximation of a constant heat release per unit mass. Thus, the temperature ratio ( $\theta \equiv T_0/T_2$ ) might, as a first rough approximation, be assumed constant and assigned a time-independent value in the vicinity of  $\theta = 0.1$ . With these final approximations, which really are neither needed nor used in part of the development, the density  $\rho_1$  is constant, while  $\rho_2 = p\theta\rho_0$  ( $p \equiv p_1/p_0$ ) varies with time in proportion to  $p$ .

It should be emphasized that the severe approximations defined in the preceding paragraph are amenable to improvement in various ways. For example,  $\theta$  could be treated as a function of  $p$  instead of being assigned a constant value. A particular variation of this type is  $k\theta p = \text{constant}$ , which corresponds to a constant temperature ratio across the flame; it seems likely that the time variation of  $\theta$  would lie between the variation predicted by this formula and that corresponding to the assumption  $\theta = \text{constant}$ . Consequences of alternative assumptions such as  $k\theta p = \text{constant}$  will not be investigated since it is felt that the adopted approximations are sufficient for a first, qualitative study. However, in employing results of the present analysis, one should be sure to realize that according to normal-shock tables,  $k$  does in fact vary with  $p$ . Larger values of  $1/k$  must be employed for larger values of  $p$ . It is, of course, possible to treat  $k$  as an explicit function of  $p$ , defined by normal-shock relations. Such an approach would have the advantage of building in an approximately realistic time variation of  $k$  from the outset. It would have the disadvantage of complicating the formulas and of introducing an additional parameter (the ratio of specific heats,  $\gamma$ ). Therefore, to preserve simplicity, explicit variations of  $k$  are not introduced. While this does not compromise these results which are independent of the assumption that  $k = \text{constant}$ , it does indicate that more refined analyses would be of interest for further testing of many results.

The assumptions outlined above form the basis of a qualitative analysis of the dynamics of motion of the shock and the flame in the cloud. Indeed, this shock itself can cause structural damage if it is strong enough; detonation is not essential for the combustion of a cloud to be of practical concern. For this reason, the flame-generated blasts defined here have been termed non-ideal explosions. Thus, the objective of the following presentation is development of an approximate analysis of non-ideal explosions. The ultimate aim is two-fold; first, to obtain an estimate of the severity of the non-ideal explosion and second to define conditions needed for the non-ideal explosion to evolve into a detonation.

The forms of the overall conservation equations to be used in describing non-ideal explosions will depend on the geometry of the cloud and the position of flame initiation. Three potentially important cases can be visualized, viz., a spherically symmetrical system with no boundaries, a hemispherically symmetrical system with a noncombustible gas in one half-space, and a cylindrically symmetrical system in which the cloud is bounded by a rigid wall (water) on one side and a gas (air) on the other. These three cases are analyzed sequentially as follows.

### Spherical Symmetry

Let the shock be located at radius  $R$  and the flames at radius  $r$ . There are three basic conservation equations to be considered. One is momentum conservation across the shock wave. This can be written as

$$p_1 - p_0 = \rho_0 V^2 (1 - \rho_0/\rho_1), \quad (1)$$

where  $V \equiv dR/dt$ . Mass conservation across the shock has been used to derive the term involving  $\rho_0/\rho_1$ .

The second condition is overall mass conservation for the sphere of radius  $R$ . This is

$$\rho_2 r^3 + \rho_1 (R^3 - r^3) = \rho_0 R^3 . \quad (2)$$

The left-hand side of Eq. (2) is the sum of the mass contained in the core of burned gases and that contained in the shocked, unburned shell around it (aside from a factor  $4\pi/3$ , which has been cancelled). The right-hand side is the mass contained in the sphere prior to initiation of the process; since the exterior of this region has been unaffected by the explosion, the shock and flame can merely have redistributed the mass that was originally present in the interior.

The third condition is mass conservation for the burned core. This is expressed as

$$r^2 \rho_1 S = (d/dt) (1/3 r^3 \rho_2) , \quad (3)$$

where a factor of  $4\pi$  has been cancelled. Equation (3) relates the mass consumption rate of the flame to the rate of core growth.

The equations can be non-dimensionalized, although this is not really necessary. For convenience, we take the initial shock radius ( $R_0$ ) as the unit of length, and we define  $x \equiv r/R_0$ ,  $y \equiv R/R_0$ . The Newtonian sound speed of the undisturbed gas, viz.,  $a \equiv p_0/\rho_0$ , is taken as the unit of velocity in defining the non-dimensional time  $\tau \equiv at/R_0$ . We also let  $s \equiv S/a$ . Then, from these along with previous definitions, we obtain

$$p = 1 + (1 - k) (dy/d\tau)^2 , \quad (4)$$

$$\theta p x^3 + (y^3 - x^3)/k = y^3 , \quad (5)$$

and

$$x^2 s/k = (d/d\tau) (\theta p x^3/3) . \quad (6)$$

Our first objective is to investigate the character of the solutions to this set of equations. It may be emphasized that in deriving Eqs. (4), (5), and (6), the possibility of time variations of  $k$  and  $\theta$  has been included.

A variety of facts may be noted. Differentiating Eqs. (1) or (4) shows that the sign of  $dp/d\tau$  is the same as the sign of  $d^2y/d\tau^2$ . Thus the shock accelerates for  $dp/d\tau > 0$  and decelerates for  $dp/d\tau < 0$ . The solutions which concern us most are non-deceleratory, and therefore we emphasize cases in which  $dp/d\tau > 0$ .

In addition, we are concerned only with cases in which  $y > x$ . Since Eq. (5) can be written in the form

$$y(1 - k)^{1/3} = x(1 - k\theta p)^{1/3} , \quad (7)$$

it is clear that this requires  $\theta p < 1$ , which states that  $\rho_2 < \rho_0$ . Stated differently, since the shell density exceeds atmospheric density, the core density must be less than atmospheric for a mass balance to be achieved in which the shock is outside the flame. It may be worth emphasizing that on the basis of additional physical considerations, further conditions arise which can be more restrictive than this.

According to Eq. (3), if the core density remains constant, the flame speed differs from  $dr/dt$ . In this case, we find from Eq. (6) that  $s = k\theta p \, dx/d\tau$ , and since  $k\theta p = \rho_2/\rho_1 < 1$ , the rate of expansion of the core exceeds the flame speed. This, of course, is due to the low core density. Typically  $\theta = \text{constant}$  and  $dp/d\tau > 0$ , so Eq. (6) shows that  $s = k\theta p \, dx/d\tau + (k\theta x/3) \, dp/d\tau$ , which tends to bring  $s$  closer to  $dx/d\tau$ , through compression of the core. However, this compression effect is unlikely to decrease the rate of expansion of the core down to the flame speed; the needed acceleration of the shock is too high to evolve naturally from a spark or flame ignition.

It is interesting to compare the rate of core expansion with the rate of shock propagation. Writing Eq. (7) in the form  $p = [1 - (y/x)^3 (1 - k)]/(k\theta)$ , we see that when  $k$  and  $\theta$  are approximately constant, if the ratio  $y/x$  increases with time then  $p$  must decrease with time. Since we are interested in  $dp/d\tau > 0$ , it is seen that we are faced with cases in which the ratio  $y/x$  either remains constant or decreases with time. Thus,  $dy/d\tau < (y/x) \, dx/d\tau$ , and since supersonic<sup>3</sup> shock propagation requires that  $dy/d\tau > 1$ , the rate of core expansion is bounded from below by the ratio  $x/y < dx/d\tau$ . The ratio  $x/y$  remains constant for a simple similarity solution, as seen below. The present observations imply that in the nonsimilar case, to have  $dp/d\tau > 0$  it is necessary to begin with a condition such that  $y/x (= 1/x_0)$  exceeds its similarity value. Then as time goes on,  $y/x$  will decrease, approaching the similarity value. Had the initial condition been such that  $1/x_0$  were less than the similarity value, then  $dp/d\tau$  would initially be negative,  $y/x$  would increase with time, and the solution again would tend to approach similarity. Thus the similarity solution appears to represent the stable, long-time, limiting behavior of the system, approached irrespective of the specific initial conditions. It should be emphasized that in this particular reasoning,  $k$  and  $\theta$  have been treated as constants. Nevertheless, it is believed that variations in these quantities typically are small enough for the conclusion to be correct, qualitatively, that the time-dependent evolution tends to approach similarity.

The similarity solution may be obtained by assuming that  $y/x$  is constant. With  $k$  and  $\theta$  presumed constant, Eq. (7) then implies that  $p$  is constant. According to Eq. (4), this requires  $dy/d\tau$  to be constant, which in turn (since  $y/x$  is constant) requires  $dx/d\tau$  to be constant. This final result is consistent with Eq. (6), if  $s$  is constant. From Eq. (6) one obtains  $s = k\theta p \, dx/d\tau$ , from Eq. (7)  $dx/d\tau = (dy/d\tau)(1 - k)^{1/3}/(1 - k\theta p)^{1/3}$ , and from Eq. (4)  $dy/d\tau = \sqrt{(p - 1)/(1 - k)}$ , resulting in

<sup>3</sup>The value of  $dy/d\tau$  is unity if the shock speed equals the Newtonian sound speed, but  $\gamma$  if the shock speed equals the isentropic sound speed (the physically correct limit). To avoid introducing the additional parameter  $\gamma$ , the Newtonian speed is used throughout. Resulting bounds all remain applicable. In some cases, conditions that are even more restrictive can be obtained by introducing  $\gamma$ .



$$s = k\theta p \sqrt{p - 1} / [(1 - k\theta p)^{1/3} (1 - k)^{1/6}] \quad (8)$$

as an expression determining  $p$  in terms of  $s$ ,  $k$ , and  $\theta$  for the similarity solution. It appears that the characteristic time for this solution to be approached is  $R_0/a$ , and the solution will remain a good approximation even if  $s$ ,  $k$ , or  $\theta$  vary with time, so long as the characteristic time scale for the variation is appreciably longer than  $R_0/a$ . Thus, the similarity solution emerges as being surprisingly useful in practice.

In view of this apparent utility, Eq. (8) has been used to calculate numerical values of the dependence of shock strength on flame speed. Results are given in Table B-1 and plotted in Figure B-1. These results may be employed in estimating damage produced by non-ideal explosions. The pressure ratio increases with increasing flame speed and also with increasing heat release. In addition, larger density ratios across the shock favor larger pressure ratios. Typically, the pressure ratio becomes substantial (e.g., a factor of two) when the Mach number of the flame (based on the Newtonian sound speed of the undisturbed atmosphere) reaches about 0.1, i.e., for a flame speed of about 20 m/sec. A flame speed of 1 m/sec produces a pressure rise across the shock of about 10%.

A number of points deserve to be mentioned in connection with Figure B-1. First, strictly speaking the results are applicable only for the similarity solution; at best, they can provide only estimates under nonsimilar conditions. Second, provided that similarity is attained, the user is free to employ any desired dependence of  $k$  and  $\theta$  on  $p$  and  $s$ ; for example, it surely is reasonable to select values for  $k$  which decrease as  $p$  increases (e.g., as predicted by normal shock relations). When this last selection is made, it is found that  $(\partial^2 p / \partial s^2)_\theta > 0$  (whereas the figure shows that  $(\partial^2 p / \partial s^2)_{\theta,k} < 0$ ). Kuhl, Kamel, and Oppenheim have accounted for a nondimensional pressure at the flame,  $p_f \equiv p_2/p_0$ , exceeding the pressure ratio across the shock,  $p_s \equiv p_1/p_0$ ; when normal-shock relations for  $k$  are used to specialize the present results to a case  $k\theta p = 1/7$ , which they considered in their Figure 11, it is found that  $p_s < p < p_f$ , as one might expect (i.e., for any specified flame speed, the present model yields a value for the pressure in region 1 lying between the pressure behind the shock and the pressure at the flame, calculated from the more precise theory). Third, there are bounds beyond which the curves in Figure B-1 do not correspond to physically attainable conditions. The restriction  $\theta < 1/p$  has been mentioned previously. The condition  $dy/d\tau > 1$  introduces the lower bound on  $p$  shown in the figure. Since supersonic shock propagation requires that  $dy/d\tau > \gamma$ , the real bound corresponding to this condition is slightly more severe than that drawn (e.g., for  $k = 1/4$  it is  $p = 2.05$  if  $\gamma = 1.4$ ); real lower bounds are not shown because a series of lines would be needed for different values of  $\gamma$ . Finally, for steady flame propagation there is an upper bound for  $s$ , defined by the lower Chapman-Jouguet point. Since this upper bound depends on two parameters,  $\gamma$  and the nondimensional heat release, it has not been indicated in the figure. However, it may be stated that, provided the flame is not accelerating, values of  $s$  as large as roughly 0.5 are not likely to be encountered.

TABLE B-1. Dependence of Nondimensional Flame Speed (s) on Shock Strength (p).

$p_0$	0.05	0.1	0.15	0.2	0.3	0.5
<u>s for k = 1/4</u>						
1.01	.001330	.00267	.00402	.00539	.00816	.01385
1.1	.00458	.00921	.01388	.01860	.0282	.0479
1.2	.00707	.01422	.0214	.0287	.0436	.0743
1.5	.01399	.0282	.0425	.0571	.0868	.1491
2	.0264	.0534	.0808	.1087	.1661	.289
3	.0563	.1142	.1737	.235	.363	
5	.1340	.274	.422	.577		
10	.411	.866				
15	.789					
<u>s for k = 1/2</u>						
1.01	.00286	.00577	.00873	.01175	.01796	.0312
1.1	.00986	.01990	.0301	.0406	.0622	.1087
1.2	.01521	.0308	.0466	.0629	.0965	.1696
1.5	.0302	.0611	.0929	.1257	.1944	.348
2	.0571	.1163	.1777	.242	.379	.707
3	.1222	.251	.389	.536	.872	
5	.293	.618	.985	1.414		
10	.927	2.12				
15	1.842					
<u>s for k = 2/3</u>						
1.01	.00364	.00737	.01120	.01512	.0233	.0413
1.1	.01256	.0255	.0387	.0523	.0809	.1445
1.2	.01940	.0394	.0599	.0811	.1258	.227
1.5	.0385	.0784	.1198	.1630	.256	.477
2	.0730	.1496	.231	.316	.507	1.029
3	.1567	.326	.511	.718	1.232	
5	.379	.817	1.348	2.06		
10	1.225	3.09				

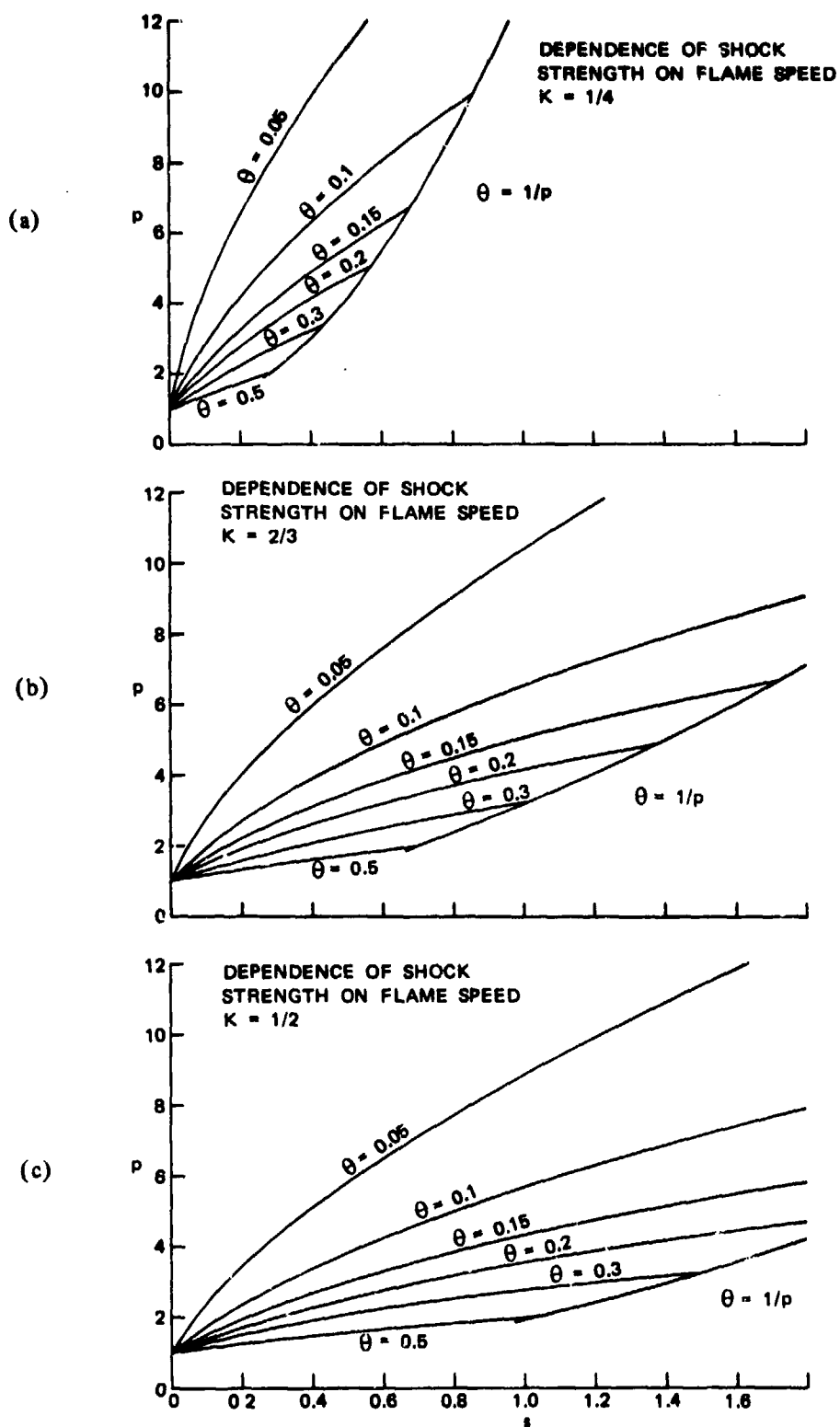


FIGURE B-1. Dependence of Shock Strength on Flame Speed.

### Hemispherical Symmetry

This problem differs from that just treated in that a half-space is occupied by a noncombustible gas. The shock is still assumed to be spherical, with radius  $R$ . However, the flame is hemispherical, and it again is assigned radius  $r$ .

Momentum conservation across the shock remains unchanged, being given by Eq. (1). The overall mass conservation condition acquires the modified form

$$[(\rho_1 + \rho_2)/(2)]r^3 + \rho_1(R^3 - r^3) = \rho_0 R^3, \quad (9)$$

since the burned core now is hemispherical, the other half of the central sphere being occupied by noncombustible shocked gas of density  $\rho_1$ . The conservation equation for a consumption of material by the flame will still be given by Eq. (3), the result being derived by considering a balance for a hemisphere rather than a sphere. Thus, in total it is seen that the equations are quite similar to those for the previous case.

Equations (4) and (6) may still be derived, but Eq. (5) is replaced by

$$[(\theta p/2) + (1/2K)] x^3 + (1/k)(y^3 - x^3) = y^3. \quad (10)$$

Equation (10) changes Eq. (7) into

$$y(1 - k)^{1/3} = x(1 - k\theta p)^{1/3}/2^{1/3}, \quad (11)$$

the factor  $1/2^{1/3}$  accounting for the modified geometry. It is clear that the character of the solutions will not differ qualitatively from that discussed in the previous case. However, there are important quantitative differences.

The requirement  $y > x$  no longer translates into  $\theta p < 1$ ; instead, the more restrictive condition  $\theta p < 2 - 1/k$  is obtained from Eq. (11). Before providing a restriction on  $\theta p$ , this condition imposes a requirement on  $k$ , viz.,  $k > 1/2$  (i.e.,  $\rho_1 < 2\rho_0$ ). This restriction clearly is essential from overall mass conservation; if it were violated, then the density of the burned core would have to be negative to maintain the overall mass balance. The ultimate result is a severe restriction on the intensity of the shock. To understand this, observe that in the simplest interpretation (and implicit in Eq. (1), for example) the quantity  $1/k$  represents the density ratio across the shock. According to normal shock tables for  $\gamma = 1.4$ , the restriction  $k > 1/2$  then translates into a shock Mach number less than 1.58 and a pressure ratio  $p$  less than 2.75.

There are two effects which tend to modify the severity of this restriction. The first is the spatial variation of density behind the shock (if the shock speed is constant, due to flame-produced compression after shock passage, then in reality  $\rho_1$  will not be constant but instead will increase as the radial distance to the point in question decreases). This implies that the value of  $k$  appearing in Eq. (1) (i.e., the average value of  $k$  in region 1) is somewhat less than the density ratio across the shock. Thus, the shock must be even weaker than estimated above. A rough estimate suggests that this phenomena tends to modify the shock-strength restriction to roughly  $p < 2$ .

On the other hand, with the driving flame present only in a half-space, it is likely to be incorrect to assume that the shock is spherical. The shock is expected to be weaker in the noncombustible gas, and consequently a smaller volume will be influenced in this half-space. This effect can be formally introduced by defining an efficiency ( $\eta$ ) as the ratio of the volume of noncombustible to combustible half-space contained within the shock. Equation (9) then takes on the revised form

$$\rho_2 r^3 + \rho_1 (R^3 - r^3) + \eta \rho_1 R^3 = \rho_0 R^3 + \eta \rho_0 R^3, \quad (12)$$

and Eq. (11) becomes

$$y(1 - k)^{1/3} = x(1 - k\theta p)^{1/3}/(1 + \eta)^{1/3}. \quad (13)$$

The restriction  $y > x$  becomes  $\theta p < 1 + \eta - \eta/k$ , and the condition of  $k$  is modified to  $k > \eta/(1 + \eta)$ , which is less severe than  $k > 1/2$  if  $\eta < 1$ . A proper calculation of  $\eta$  entails solving for the nonspherical flow field. A reasonable estimate could be  $\eta = 1/2$ , in which case the shock-strength restriction becomes  $k > 1/3$ , or a Mach number less than 2.23,  $p < 5.64$  (for  $\gamma = 1.4$ ). Considering all of the corrections together, one might estimate that  $p < 3$  is a definite upper limit. Obviously, the presence of the free boundary can severely reduce the intensity of the shock.

This particular result appears to be the most important one obtained from the present study. Therefore, its reasonable generality seems to be worth emphasizing. No assumptions have been made that either  $k$  or  $\theta$  are independent of time, nor has a similarity hypothesis been introduced. Nothing more than overall balances have been involved. It is time to define a wave-pattern efficiency  $\eta$ . While this appears to be a useful crutch to enhance physical comprehension, assuredly it is a highly approximate way to describe the complex pattern of waves in the noncombustible gas. A correct description of the wave pattern necessitates integration of partial differential equations. This is beyond the scope of the present study and apparently has not been accomplished previously by other investigations for the hemispherical geometry (or for the cylindrical geometry defined in the next section). Thus, there appears to be no better theory against which the present predictions can be checked. The estimate of  $\eta$  given above is purely intuitive; it is possible that  $\eta$  is very near zero, so that the limitation on  $p$  for the non-ideal explosion is not at all severe. However, tendencies for detonations to decay when propagating in media bounded by noncombustible gases have been observed experimentally. In view of this fact, it does not seem unreasonable to suggest that the less intense reactions, which are associated with non-ideal explosions, will be subject to stringent bounds on shock intensity in unconfined systems.

Aside from the restriction on shock intensity, the system dynamics are quite similar to the previous case. In particular, within the context of the global description that has been introduced, there still exists a similarity solution which tends to be approached rapidly as time goes on, irrespective of the initial conditions. The relationship between flame speed and shock strength for the similarity solution, derived in the same way as Eq. (8), is

$$s = k\theta p \sqrt{p - 1} (1 + \eta)^{1/3} / [(1 - k\theta p)^{1/3} (1 - k)^{1/6}] . \quad (14)$$

This equation allows Table B-1 and Figure B-1 to be used for the hemispherical case as well, merely by replacing  $s$  with  $s/(1 + \eta)^{1/3}$ . It is seen from this result that the flame speed needed to produce a given pressure ratio is larger by the factor  $(1 + \eta)^{1/3}$  in the hemispherical case. For  $\eta = 1$  this corresponds to a 25% increase in the required flame speed. Since this is not a very large increase, it may be concluded that the major effect of the hemispherical geometry is limitation of the shock intensity.

### Cylindrical Symmetry

Here we assume that a cloud of height  $h$  is bounded below by a rigid wall and above by a noncombustible gas. The flame is viewed as a right circular cylinder of radius  $r$  and height  $h$ , and within the cloud this same shape is assigned to the shock, with radius  $R$  and height  $h$ . In the simplest model, a hemispherical shock of radius  $R$  will exist in the noncombustible gas. In keeping with the ideas introduced in the previous section, we shall employ an efficiency  $\eta$ , such that the actual volume subtended by the shock in the noncombustible is  $\eta$  times the volume of this hemisphere.

Equation (1) remains valid, but Eq. (2) is replaced by

$$\rho_2 r^2 h + \rho_1 (R^2 - r^2) h + (2/3) \eta \rho_1 R^3 = \rho_0 R^2 h + (2/3) \eta \rho_0 R^3 . \quad (15)$$

Equation (3) also changes, now becoming

$$r \rho_1 S = (d/dt) (1/2 r^2 \rho_2) . \quad (16)$$

In nondimensional form, we now have Eq. (4), along with

$$\theta p x^2 + 1/k (y^2 - x^2) + 2/3 \eta/\alpha (1/k - 1) y^3 = y^2 \quad (17)$$

and

$$xs/k = (d/d\tau) (\theta p x^2/2) . \quad (18)$$

The nondimensional cloud height has been defined as  $\alpha \equiv h/R_0$ . Equations (17) and (18) differ from Eqs. (5) and (6) first in the presence of squares instead of cubes and second in the presence of the term involving  $\eta/\alpha$ .

The squares would introduce no important difference from the behavior discussed for the spherical case. In particular, the similarity solution would still be obtained. Cube roots would become square roots and would have the effect of intensifying the pressure wave for a specified flame speed (e.g., Eq. (8) would become  $s = k\theta p \sqrt{p - 1/\sqrt{1 - k\theta p}}$ ). The  $\eta/\alpha$  term, however, modifies the results significantly. In addition to providing a loss effect which tends to reduce  $p$ , it destroys similarity by introducing  $y^3$ .

This qualitative influence of the  $\eta/\alpha$  is comprehensible. As time increases then the  $\eta/\alpha$  term becomes proportionally larger than the others. Thus, the loss becomes increasingly important with increasing time and causes the shock to decay. This is because when  $\eta$  is fixed, the volume of the noncombustible gas intercepted by the shock increases more rapidly than the volume of the combustible gas. The smaller the cloud height  $h$  (i.e., the smaller the  $\alpha$ ), the larger will be the loss effect. At early times, if  $h \gg R_0$  (i.e., if  $\alpha \gg 1$ ) then the loss effect is negligible and the shock may be expected to be stronger than in the spherical case. However, this situation appears unlikely to occur in LNG spills; initiation is likely to occur at a point, and the cylindrical model will become applicable only after  $R > h$ . Thus, in practice, the  $\eta/\alpha$  must be significant for the model to be correct. Clearly, the non-ideal explosion in this cylindrical case potentially becomes appreciably weaker than it is in either of the other two cases.

It is not obvious that the efficiency  $\eta$  will remain constant in time. As the diameter of the shock cylinder increases, the volume of the intercepted noncombustible gas above the cylinder may well increase more slowly than the cube of the diameter. Analysis of the evolution of the nonsymmetrical shock pattern is needed to see how large this effect may be. It seems highly unlikely that the effect could be great enough to eliminate decay. However, the presence of the effect does suggest that a reasonable idea of the dynamics of the system can be obtained by treating  $\eta y \equiv \mu$  as a constant for short periods of time.

When the substitution  $\eta = \mu/y$  is made, Eq. (17), the nature of the dynamics becomes clear through comparison with the previous cases. A similarity solution again emerges, and the system, when removed from this solution, tends to approach it quite rapidly (time scale  $R/a$ ). The general relationship between  $y$  and  $x$ , obtained from Eq. (17), is

$$y(1 - k)^{1/2} = x(1 - k\theta p)^{1/2} / (1 + 2/3 \mu/\alpha)^{1/2}, \quad (19)$$

which may be compared with Eq. (13). The same type of restriction on shock strength, derived in the previous section, emerges here; the correspondence being exact if  $\eta$  of the previous section is identified with  $2/3 \mu/\alpha$  (i.e.,  $2/3 \eta y/\alpha$ ) of the present section. It is evident that, especially for large values of  $y$ , the maximum shock strength is appreciably less for the cylindrical case than for the hemispherical case.

Following the procedure of the previous section, normal shock tables for  $\gamma = 1.4$  were used to obtain an upper bound for the shock strength, as a function of the shock radius  $R$ , cloud height  $h$ , and efficiency  $\eta$ . The results, given in Table B-2, show that even for  $\eta$  as small as 0.1, the pressure increase across the shock will not exceed 20% at a distance of 1,000 meters from the initiation point in a typical LNG cloud.

The relationship between flame speed and shock strength, obtained as before, is

$$s = k\theta p \sqrt{p - 1} \sqrt{1 + 2/3 \eta y/\alpha} / \sqrt{1 - k\theta p} \quad (20)$$

TABLE B-2. Maximum Shock Strength for Cylindrical Case.

$2\eta R/3h$	p
0.25	29.0
0.35	10.3
0.40	8.03
0.48	6.00
0.60	4.50
0.90	3.00
1.60	2.00
2.93	1.51
6.58	1.22
11.91	1.12
29.90	1.05
60.10	1.02



for the similarity solution. The factor involving  $\eta/\alpha$  necessitates a higher flame speed for achieving a given pressure ratio.

### Conclusion

A non-ideal explosion could produce a damaging pressure wave over distances of the order of magnitude of the LNG cloud height; but for distances greater than roughly ten times this height, the shock should be expected to weaken, irrespective of the diameter of the cloud. Unless a transition to detonation occurs, severe blast damage will not extend over large distances.

### TRANSITION TO DETONATION

There are two basically different mechanisms whereby a detonation can develop from a non-ideal explosion. One involves acceleration of the flame until it overtakes the shock. This acceleration is a complex phenomenon and is likely to depend on pre-existing turbulence as well as flame-produced turbulence. It is possible to introduce hypotheses concerning flame acceleration and to feed the results into the model of the previous section. This approach will be discussed first, without considering potential mechanisms of flame acceleration.

The second mechanism is the occurrence of a homogeneous thermal explosion in the shock-heated cloud ahead of the flame. This process can be treated with somewhat greater accuracy and will be considered second.

Comments on some potential mechanisms for flame acceleration will then be given.

### Flame Acceleration

Equations (4), (5), and (6), for example, imply that if  $s(\tau)$  is specified then a nonlinear second-order differential equation exists for  $y(\tau)$ . With  $k$  and  $\theta$  taken as constants, this equation is

$$\frac{2}{3}(1-k)y(dy/d\tau)(d^2y/d\tau^2) = [1 - k\theta - k\theta(1-k)(dy/d\tau)^2] \left\{ (s/k\theta) \left[ \frac{1 - k\theta - k\theta(1-k)(dy/d\tau)^2}{1-k} \right]^{1/3} - [1 - (1-k)(dy/d\tau)^2] (dy/d\tau) \right\}$$

and its initial conditions are  $y = 1$ , and  $dy/d\tau = \sqrt{[1 - (1-k)/x_0^3] - k\theta}/[k\theta(1-k)]$  at  $\tau = 0$ . The problem defined here is quite complex and requires numerical integration by means of a computer. If such an integration is preferred, it would be of interest to include, as well, reasonable time variations of  $k$  and perhaps of  $\theta$ . In the absence of numerical integrations, it is difficult to draw accurate conclusions concerning the functions  $s(\tau)$  which are needed to cause  $x(\tau)$  to approach  $y(\tau)$ . However, a few general observations can be made.

In view of the existence of the similarity solution and the tendency of solutions to approach it, it would seem to be difficult to cause the flame to overtake

the shock. For example, if initial conditions are reasonably close to similarity, then appreciable flame acceleration over a time scale comparable with  $R/a$  (acoustic time) would be needed to perturb the system from near-similarity. Substantial initial departure from similarity could be essential.

The flame will tend to overtake the shock only if  $dx/d\tau > dy/d\tau$ . Necessary conditions for this to occur can be derived from Eqs. (4) through (7). Differentiation of Eq. (7) shows that if  $k$  and  $\theta$  are constant then

$$(dy/d\tau) = (y/x)(dx/d\tau) - (k\theta/3) y [(dp/d\tau)/(1 - k\theta p)] , \quad (21)$$

from which it immediately follows that  $dp/d\tau > 0$  is necessary. Use of this result in the derivative of Eq. (4) then shows that  $d^2y/d\tau^2 > 0$  also is necessary. Overtaking can occur only under conditions that are accelerating in all respects.

From Eqs. (21) and (6) it follows that

$$(dy/d\tau) = (y/x)(dx/d\tau) - [(3s/k\theta x) - (3p/x)(dx/d\tau)] (k\theta/3) y/(1 - k\theta p) ,$$

which reduces to

$$(dx/d\tau) = s + (1 - k\theta p) (x/y) (dy/d\tau) . \quad (22)$$

Equation (22) implies that

$$(dx/d\tau) - (dy/d\tau) = s - [1 - (1 - k\theta p) (x/y)] (dy/d\tau) ,$$

which provides a bound on  $s$  needed for overtaking, viz.,

$$s > [1 - (1 - k\theta p)[(1 - k)/(1 - k\theta p)]^{1/3} \sqrt{(p - 1)/(1 - k)} \quad (23)$$

where use has been made of Eqs. (4) and (7). For  $\theta p \ll 1$  and  $k$  not too large, this bound becomes approximately  $s > (k/3)\sqrt{(p - 1)/(1 - k)}$ . The restriction typically is significant, requiring the flame speed to be an appreciable fraction of the sound speed.

### Thermal Explosion

A physically logical mechanism for detonation development is as follows. The flame generates the shock, which in turn heats the combustible gas passing through it. Initiation reactions begin to occur in the heated gas. The rates of these reactions depend strongly on temperature. The temperature history experienced by the heated element therefore determines the extent of the reaction occurring within it. If the temperature history is such that sufficient reaction occurs to cause ignition prior to arrival of the flame, then a "thermal explosion" generates a new flame ahead of the original one. The process then rapidly accelerates through formation of additional new flames, and the ideal explosion develops quickly.

It may be noted that calculation of detonation development on the basis of this model does not require consideration of an accelerating initial flame; the similarity solution developed previously will do nicely. The additional physical input needed is the ignition time of the fuel cloud as a function of temperature. Data of this type are available for numerous fuels (see, for example, Penner, S. S. and Mullins, P. B., *Explosions. Detonation, Flammability, and Ignition*, AGARD-O-graph, No. 31, Pergamon, 1959). Because of the strong temperature dependence of the ignition time, it is desirable to account for temperature change of fuel elements behind the shock through adiabatic compression. The previous model can be used with such a temperature history grafted onto it. However, to obtain a first rough estimate, the temperature changes will not be introduced here.

The available data appear as ignition time,  $\tau_{ig}$ , versus temperature. Presuming that the ignition reaction can be approximated in the form

$$dY/dt = -Y/\tau_{ig} ,$$

where  $Y$  is a normalized reactant concentration and presuming that  $Y$  goes from 1 initially to 0 at ignition, the ignition requirement may be expressed generally as

$$\int_0^t (dt/\tau_{ig}) = 1 , \quad (24)$$

where the integral is carried over the time history of a fuel element. In the cloud, let us assume that the temperature behind the shock is the constant value  $T_1$ . Then Eq. (24) immediately gives, as a condition for detonation development,

$$\tau_{ig} (T_1) = \Delta t , \quad (25)$$

where  $\Delta t$  is the time between arrival of the shock and arrival of the flame.

The ignition time is correlated by an Arrhenius expression

$$\tau_{ig} = e^{E/R^\circ T/A} , \quad (26)$$

where  $A$  is a pre-exponential factor and  $E$  an activation energy. For methane,  $E = 29$  kcal/mole (Mullins). Also for methane,  $\tau_{ig} = 100$  msec at  $T = 800^\circ\text{C}$  (Mullins). This is longer, typically by an order of magnitude, than  $\tau_{ig}$  for most other fuels at this temperature. Also, the activation energy for methane is on the low side of the representative range (40 to 60 kcal/mole). Thus, at higher temperatures methane is relatively even more difficult to ignite.

Normal shock tables were used to calculate  $\Delta t$  required for ignition of methane as a function of shock strength  $p$  (assuming  $\gamma = 1.4$  and  $T_o = 300^\circ\text{K}$ ). The results are listed in Table B-3. It is seen that rather strong shocks, e.g.,  $p = 10$ , are needed to produce ignition in 1 second.

The time available between shock arrival and flame arrival may be estimated from the similarity solution. We obtain

**TABLE B3. Ignition Time for Methane as a Function of Shock Strength.**

p	$\Delta t$ (msec)
1.02	$1 \times 10^{17}$
1.05	$7 \times 10^{16}$
1.12	$3 \times 10^{16}$
1.22	$9 \times 10^{15}$
1.51	$5 \times 10^{14}$
2.00	$2 \times 10^{13}$
3.00	$8 \times 10^{10}$
4.50	$4 \times 10^8$
6.00	$8 \times 10^6$
8.03	$2 \times 10^5$
10.3	$1 \times 10^3$
29.0	$6 \times 10^{-1}$

$$\Delta t = (R/a) / \sqrt{(1-k)/(p-1)} \left\{ \left[ 1 - \left( (1-k)/(1-k\theta p) \right)^{1/3} \right] / \left[ \left( (1-k)/(1-k\theta p) \right)^{1/3} - (1-k) \right] \right\} \quad (27)$$

The typical order of magnitude of  $\Delta t$  is  $R/a$ . For a cloud 1,000 meters in diameter, this corresponds to a time  $\Delta t$  of a few seconds. Thus, in such a cloud the rather large value of  $p \approx 10$  is needed for detonation.

The value of  $\Delta t$  required for detonation increases so rapidly with decreasing shock strength that extremely large clouds ( $10^{10}$  meters) are needed for this mechanism to produce an ideal explosion for moderate pressure waves ( $p = 2$ ). Moreover, under these low temperatures, methane should ignite about as easily as other fuels. Thus, the thermal explosion mechanism should not be very important unless the non-ideal explosion itself is very strong.

### Acceleration Mechanisms

Since thermal explosion does not appear to be a viable mechanism of transition to detonation, it appears that mechanisms for substantial flame acceleration must be found if development of a detonation is to be described. Since the distant shock, per se, is not likely to influence the flame dynamics substantially, the flame acceleration may be sought without considering the shock explicitly. R. A. Strehlow, of the Department of Aeronautical and Astronautical Engineering, University of Illinois, has defined four potential mechanisms for flame acceleration. These are (1) an acceleration-wave (Taylor) instability of the flame, (2) interaction of the flame with a turbulent bounding layer on a flat surface, (3) impingement of the flame on obstacles and interaction of the flame with the turbulent flow thereby generated, and (4) propagation of the flame into a confined space, with subsequent development of detonation within the confinement, followed by propagation of detonation out of the confinement, into the cloud. Mechanisms (1) and (2) may occur even over open water, while mechanisms (3) and (4) require the presence of rigid structures (ships, shore contours, or buildings on shore). From earlier studies, it seems certain that mechanism (4) is viable; a sufficiently long confinement can generate a detonation which would propagate through the cloud. Mechanism (3) should also be viable for obstacles of suitable size, shape, and placement; currently insufficient information is available to define the required configurations of obstacles. At present, it is unknown whether mechanisms (1) and (2) can in fact generate detonations. Each of these two mechanisms is amenable to approximate theoretical analysis, but the analyses have not been performed.

In considering mechanisms (1) and (2), it is important to keep in mind the previously derived fact that accelerations over a time scale comparable with acoustic time are needed for detonation development. For acceleration waves, the growth time is of the order of  $1/g$ , where  $l$  is the scale of the instability and  $g$  is the acceleration of the interface between light and heavy fluids (not flame). Some acceleration of the flame must be present initially for this instability to develop, and the greater the initial acceleration, the greater will be the rate of development. Atmospheric turbulence within the cloud, for example, provides some initial acceleration locally. However, it is not clear whether these small accelerations can produce sufficiently rapid growth rates for detonation development. Theoretical analyses are needed for resolving the question.

Similarly, it is not clear how sufficiently rapid accelerations could arise from interaction between the flame and boundary layer; again, theoretical analyses are needed.

One may conclude from these rough considerations that the presence of obstacles tends to enhance the probability of development of a detonation and that in the absence of obstacles it is not clear whether a detonation can develop from a non-ideal explosion.

## SUMMARY

Two major new results have been obtained from the present study. The most important is that for non-ideal explosions in the presence of an inert gas of infinite extent along one of the boundaries, there exists a limiting shock strength which depends on the efficiency of the wave pattern in the noncombustible gas. First estimates suggest that this limit can be quite severe for large LNG spills on water; decay due to upward relief lessens effects significantly at distances large compared with the cloud height. The second most important result is that the transient behavior of non-ideal explosions is such that a similarity condition of constant wave speeds tends to be approached with increasing time. Substantial flame acceleration over time scales comparable with acoustic time are needed to break away from the non-ideal explosion and to develop a detonation. It should be emphasized that both of these major results have been obtained from approximate analyses and therefore deserve to be tested by calculations of improved accuracy.

Confinement is extremely important to detonation development. Even very large clouds, when unconfined, appear to have potential difficulties in developing detonations. A major step toward safety would be to assume that LNG spills on water are far enough removed from confining obstacles (ships, etc.) that could engender development of detonation in the combustible gas. Studies of mechanisms of flame acceleration are needed for obtaining better understanding of conditions under which a transition from a non-ideal explosion to a detonation may occur. Since it appears that there are likely to exist situations in which transition to detonation does not occur, further studies of non-ideal explosions and of the damage they produce seem warranted.

APPENDIX C  
ANNOTATED BIBLIOGRAPHY

Baker, W. E., *Explosions in Air*, University of Texas Press (1973).

This is a complete textbook of the process of generation and transmission through air of blast waves from explosives.

Boyle, G. J. and A. Kneebone, *Laboratory Investigation into the Characteristics of LNG Spills on Water, Evaporation, Spreading and Vapor Dispersion*. Shell Research Limited, Released by the American Petroleum Institute, Re 6Z32, March 1973.

This is a laboratory and small scale wind tunnel investigation of the characteristics of LNG spills on water. One characteristic investigated, that has not been studied by others, is the appreciable incorporation of water in the vapor cloud.

Brossard, J., N. Manson and M. Niolet, *Propagation and Vibratory Phenomena of Cylindrical and Expanding Detonation Waves in Gases*. Transactions of the 11th Combustion Symposium, p 623, The Combustion Institute, Pittsburg, Pa., 1967.

This is a report of an investigation of the detonation of propane-oxygen-nitrogen mixtures in cylindrical segment (pie shaped) chamber. The authors observed the transition from deflagration to detonation during acceleration of the system formed by a shock wave and a combustion wave.

Burgess, D. S., J. N. Murphy and M. G. Zabetakis, *Hazards of LNG Spillage in Marine Transportation*. U. S. Coast Guard, SRC Report No. S-4105, 1970.

Burgess, D., J. Biordi and J. Murphy, *Hazards of Spillage of LNG into Water*. PMSRC Report No. 4177, U. S. Department of Interior, Bureau of Mines, Pittsburgh, Pa., 1972.

These are reports of experimental investigations of LNG spills on water. The pool spread, evaporation rate, vapor gravity spread, downwind drift and dispersion were studied in spill sizes up to 0.5 m<sup>3</sup>. In unconfined spills coherent ice flow formation was not observed. In several cases small scale physical explosions were observed but no attempt was made to study the initiation or burning of the cloud.

Edwards, D. H., *A Survey of Recent Work on the Structure of Detonation Waves*. Transactions of the 12th Combustion Symposium, p 819, The Combustion Institute, Pittsburgh, Pa., 1969.

This is a review paper that covers the structure of steady state detonation of gas mixtures in tubes. It concludes that the Zeldovich-von Neumann-Doring (ZND) model accurately predicts the macroscopic features of a detonation wave even though it does not consider the fine structure present.

Fay, J. A., *Unusual Fire Hazard of LNG Tanker Spills*. Combustion Science and Technology, 1, 47 (1973).

This report gives theoretical expressions for the pool spread and evaporation rate of liquified natural gas, spilled on water, the gravitational spread, heating and downwind spread of the vapor cloud. It does not treat the diffusion or mixing of the vapor with air.

Preceding page blank

Fields, S. F., *High Altitude Blast Generating System: Detonable Gas Mixing Experiments*. Ballistic Research Laboratories, BRL CR 95, March 1973.

This report describes the use of hydrogen-air and methane oxygen mixtures for blast wave generation.

Feldbauer, G. W., et. al., *Spills of LNG on Water-Vaporization and Downwind Drift of Combustible Mixtures*. Esso Research and Engineering Company Report No. EE61E-72, Released by the American Petroleum Institute, Re 6Z32, March 1973.

This report contains data on large (up to 10 m<sup>3</sup>) spills of LNG on water. A semi-empirical method of calculating size, concentration and downwind drift of the vapor cloud is presented.

Freiwald, H., and H. W. Koch, *Spherical Detonations of Acetylene-Oxygen-Nitrogen Mixtures as a Function of Nature and Strength of Initiation*. Transactions of the 9th Combustion Symposium, p 275, The Combustion Institute, Pittsburgh, Pa., 1963.

The spherical detonation of mixtures of acetylene-oxygen-nitrogen contained in rubber balloons of up to 1-meter diameter is reported. The detonations were initiated with flame, electric spark, hot wire, exploding wire, or the detonation of small solid explosive charges.

Kogarko, S. M., V. V. Adushkin and A. G. Lyamin, *Investigation of Spherical Detonation of Gas Mixtures*. Combustion Explosion and Shock Waves, 1, No. 2, 15, 1965.

The authors investigated the initiation of mixtures of methane and propane with air and oxygen. The ignition source was either a spark or TNT charges. The mixtures were contained in spherical rubber envelopes 0.7 to 3 inches in diameter. Both photographic and piezoelectric pressure instrumentation was used. Results are given in terms of the nature of the reaction versus the initiation strength. It was found that for a weak initiation only the propane-oxygen mixture transitioned from burning to detonation, although the flame acceleration occurred in other mixtures.

Kogarko, S. M., *Detonation of Methane-Air Mixtures and the Detonation Limits of Hydrocarbon-Air Mixtures in a Large Diameter Pipe*. Soviet Physics, 3, 1904, 1958.

The author reviews the Russian literature on methane-air detonations in tubes and describes his own work using tubes with diameters up to 0.305 meter and lengths to 12.2 meters. The gas mixtures were initiated with 50/50 amatol explosive charges. He concludes that the limits and the possibility of a detonation vary with the diameter. The limits for methane-air in the 0.305 meter tube were found to be 6.3 to 13.5% by volume methane. Methane-air mixtures could not be detonated even with strong shock initiation in small tubes (20 mm diameter).

Laderman, A. J., P. A. Urtiew and A. K. Oppenheim, *On the Generation of a Shock Wave by Flame in an Explosive Gas*. Transactions of the 9th Combustion Symposium, p 265, The Combustion Institute, Pittsburgh, Pa., 1963.

This report is a theoretical and experimental investigation of the generation of shock waves by a flame in plain geometry. The experiments consisted of observing burning fronts in hydrogen-oxygen mixtures in a rectangular cross section shock tube.

Lee, J. H., B. H. K. Lee, I. Shanfield, *Two-Dimensional Unconfined Gaseous Detonation Waves*. Transactions of the 10th Combustion Symposium, p 805, The Combustion Institute, Pittsburgh, Pa., 1965.

The authors conclude from theoretical arguments that unconfined cylindrical detonations cannot exist at small radius. Experimentally they found with mixtures of acetylene and oxygen, that with sufficiently strong initiation, over driven waves are produced that decay to a constant velocity which corresponds to the plane C-J velocity. They also observed transitions from burning to detonation when turbulence intensity was artificially increased by insertion of a spiral wire coil.



National Research Council, *Conference Proceedings on LNG Importation and Terminal Safety*. Advisory Committee on Hazardous Materials, DOT US Coast Guard Project 733211, June 1972.

This is the report of a conference held to consider all of the potential hazards of handling and shipment of LNG; however, the possibility of a detonation of a natural gas-air cloud was not discussed.

Nichols, J. A., et. al., *Fundamental Aspects of Unconfined Explosions*. Air Force Armament Laboratory Technical Report AFATL-TR-73-125, 1973.

The first part of this report is a generalized analytical prediction of the ground impulse that can be obtained from a blast wave, detonation wave, and a fuel/air explosion. The latter consists of blast wave behavior for radius less than critical radius, and C-J detonation for radius greater than critical radius. The second part of the report gives results of an experimental investigation of cylindrical detonation in fuel drop/air mixtures. Detonations in kerosene-air mixtures were observed.

Parsons, G. H., E. B. Vanta, P. M. Collins, and J. Bearly, *Techniques for Investigation of Unconfined Fuel Air Detonations*. Air Force Armament Laboratory, AFATL-TR-73-230, November 1973.

This report describes an experimental method for investigating the detonation of fuel/air mixtures in polyethylene film bags.

Soloukliin, R. I., *Nonstationary Phenomena in Gaseous Detonation*. Transactions of the 12 Combustion Symposium, p 799, The Combustion Institute, Pittsburgh, Pa., 1969.

This is a theoretical investigation of the gas dynamic structure of detonable mixtures during either transition from deflagration to detonation, or the decoupling and re-establishment of detonation that occurs close to the limits of detonability. An important conclusion is that for methane-air mixtures the ratio of effective combustion velocity to laminar flame velocity must reach 410 before transition to detonation can occur by preignition ahead of the flame front.

Strehlow, R. A., *Unconfined Vapor Cloud Explosions - An Overview*. Transactions of the 14th Combustion Symposium, p 1189, The Combustion Institute, Pittsburgh, Pa., 1973.

The author summarizes the history of accidental vapor cloud explosions, reviews the work that has been done to understand the dispersion, ignition, propagation and blast effects produced, then points out areas for future investigation.

Struck, W. G. and H. W. Reichenbach, *Investigation of Freely Expanding Spherical Combustion Waves Using Methods of High-Speed Photography*. Transactions of the 11th Combustion Symposium, p 677, The Combustion Institute, Pittsburgh, Pa., 1967.

The authors investigated spherical combustion waves in acetylene-oxygen mixtures. In the size investigated (10 cm diameter) simple transition to detonation did not occur. Detonation was produced only when the combustion wave interacted with the walls or igniter supporting structure.

The Combustion Institute, *Dynamics of the Generation of Pressure Waves by Accelerating Flames*. Transactions of the 10th Combustion Symposium, p 797, Pittsburgh, Pa., 1965.

A theoretical description of flame acceleration in spherical geometry and the generation of pressure waves ahead of an accelerating flame.

Urtiew, P. A. and A. K. Oppenheim, *Detonative Ignition Induced Shock Merging*. Transactions of the 11th Combustion Symposium, p 665, The Combustion Institute, Pittsburgh, Pa., 1967.

The authors investigated the transition from deflagration to detonation in hydrogen-oxygen mixtures with stroboscopic laser schlieren photography. They interpret the detonative ignition induced by the shock merging process ahead of the accelerating flame in terms of a kinetic induction times.

Woolfolk, R. W., *Correlation of Rate of Explosion With Blast Effects for Non-Ideal Explosions*. Stanford Research Institute, Final Report Project PRU-8056, 1971.

In this work a mixture of hydrogen and oxygen was used to simulate a non-ideal explosion. By comparing the blast wave formed by a burning mixture at various dilutions of nitrogen with the blast wave from similar mixtures that were detonated, the effect of energy release rate on blast wave propagated energy were determined. It was found that the energy propagated was dependent on the rate of energy release; the amount of energy was higher when the rate was higher.

Zabetakis, G., *Flammability Characteristics of Combustible Gases and Vapors*. Bureau of Mines, Bulletin 627, 1965.

This report is a compilation of flammability characteristics including limits of flammability, burning rate, autoignition temperature, detonation limits, and detonation rate of a variety of fuels.

## BIBLIOGRAPHY

### LNG SPILL

Burgess, D., and M. G. Zabetakis, *Fire and Explosion Hazards Associated with Liquefied Natural Gas*. U.S. Department of Interior, Bureau of Mines Report RI-6099 (1962).

Enger, T., and D. E. Hartman, *LNG Spillage on Water. I. Exploratory Research on Rapid Phase Transformations*. Shell Pipe Line Corporation, Research and Development Laboratory, Technical Progress Report 1-71, February 1971.

Enger, T., and D. E. Hartman, *LNG Spillage on Water. II. Final Report on Rapid Phase Transformations*. Shell Pipe Line Corporation, Research and Development Laboratory, Technical Progress Report 1-72, February 1972.

Enger, T., *LNG Spillage on Water. III. Spreading and Vaporization Model for an Instantaneous Spill*. Shell Pipe Line Corporation, Research and Development Laboratory, Technical Progress Report 6-72, April 1972.

Humbert-Basset, R., and A. Montet, *Dispersion Dans L'Atmosphere d'un Nuage Gazeux Forme Par Epanchage de G.N.L. Sur de Sol*. Third International Conference on Liquefied Natural Gas, Washington, D.C., September 1972.

Katz, D. L. and C. M. Sliepcevich, *LNG Water Explosions*. Hydrocarbon Processing, November 1971.

Mansillon, R., *Etude d'Accidents Hypothetiques sur un Stockage d'Hydrocarbure Refrigere a la Pression Atmospherique*. Third International Conference on Liquefied Natural Gas, Washington, D.C., September 1972.

Parker, R., and J. Spata, *Downwind Travel of Vapors From Large Pools of Cryogenic Liquids*. Proceedings of the First International Conference on LNG, April 7-12, 1968, Institute of Gas Technology, Chicago, Ill.

Williams, H. D., *Hazards of Liquefied Natural Gas in Marine Transportation*. Proceedings of the Marine Safety Council, U.S. Coast Guard, September 1971.

Williams, H. D., *More Detail on the Hazards of Liquefied Natural Gas in Marine Transportation*. Proceedings of the Marine Safety Council, Volume 29, No. 10, U.S. Coast Guard, October 1972.

Witte, S. C., and J. E. Cox, *Nonchemical Explosive Interaction of LNG and Water*. ASME Winter Annual Meeting, 28 November-2 December 1971, Washington, D.C.

## GASEOUS DETONATION

Berger, J., J. Favier, and T. Camion, *Les Ondes de Detonation*. Colloquium International C.N.R.S., Paris, 1961.

Bird, P. F., R. E. Duff, and G. L. Schott, *A Fortran Fap Code for Computing Normal Shock and Detonation Wave Parameters in Gases*. Los Alamos Scientific Laboratory, New Mexico, Report No. LA-2980, 1964.

Brossard, J. and M. Niollet, *Transfer of Energy From an Exploding Wire to a Detonating Gas*. First Colloquium (International) on Gasdynamics of Explosions, Brussels, 1967.

Cheret, R., *Fourth Symposium on Detonation*. Silver Spring, Maryland, 1965.

Dabora, E. K., J. A., Nicholls, and R. B. Morrison. *The Influence of a Compressible Boundary on the Propagation of Gaseous Detonations*. Tenth Combustion Symposium, The Combustion Institute, Pittsburgh, Pa., 1965.

Gerrard, A. J., *Methods of Flow Visualization by Means of Water*. Instrumental Methods in Combustion Research, AGARD, 1961.

Lee, J. H., R. I. Soloukhin, and A. K. Oppenheim, *Current Views on Gaseous Detonations*. First Colloquium (International) on Gasdynamics of Explosions, Brussels, 1967.

Lewis, B., and G. von Elbe, *Combustion Flames and Explosion of Gases*. Academic Press, 1961.

Litchfield, E. L., M. H. Hay, and D. R. Forshey, *Direct Electrical Initiation of Freely Expanding Gaseous Detonation Waves*. Ninth Combustion Symposium, The Combustion Institute, Pittsburgh, Pa., 1963.

Mullins, B. P. and S. S. Penner, *Explosions, Detonations, Flammability, and Ignition*. AGARD, 1959.

Oppenheim, A. K., *Gasdynamics of Explosions*. University of California, Berkeley, 1967.

Soloukhin, R. I., *Shock Waves and Detonations in Gases*. Gos. Izd. Fiz. Mat. Literatury, Moscow, 1963.

Strehlow, R. A., *The Spacing of Transverse Waves in Detonations*. First Colloquium (International) on Gasdynamics of Explosions, Brussels, 1967.

Strehlow, R. A., *Gas Phase Detonations: Recent Developments*. Combustion Flame, 1968.

Strehlow, R. A., et. al., *Transverse Wave Structure in Detonations*. 11th Combustion Symposium, The Combustion Institute, Pittsburgh, Pa., 1967.

Taylor, G. J. and R. S. Tankin. *Gas Dynamical Aspects of Detonation*. (in *Fundamentals of Gas Dynamics*) Princeton University Press, 1958.

Ubbelohde, A. R. and G. Munday, *Some Current Problems in the Marginal Detonation of Gases*. 12th Combustion Symposium, The Combustion Institute, Pittsburgh, Pa., 1969.

Zeleznik, F. J. and S. Gordon, *A General IBM 704 or 7090 Computer Program for Computation of Chemical Equilibrium Compositions, Rocket Performance, and Chapman Jouguet Detonations*. NASA Technical Note D1454, 1962.

#### FUEL-AIR EXPLOSIVES

Army Test and Evaluation Command, *Explosive Atmosphere Tests*. Aberdeen Proving Ground, Maryland, MTP-6-2-538.

Bartknecht, W., *Gaseous Explosions in Ducts (Gas Explosion in Rohrstrecken)*. Royal Aircraft Establishment, Farnborough, England, RAE-Library Trans 1240.

Berlad, A. L., C. H. Yank, and R. D. Rowe, *On Non-Adiabatic Flame Propagation*. Convair Scientific Research Laboratory, San Diego, Calif., RN-20.

Bonanno, R., *Proceedings of the Fuel-Air Explosives Conference (1st), 27-29 October 1971, Volume I, Book 2*. Air Force Armament Laboratory, Eglin Air Force Base, Florida. (AFATL-TR-71-171-Vol-1-Bk-2.)

Broekstra, G., *Note on Detonation and Blast Wave Theory, Part II, The Initial Propagation of Spherical Blast*. Defence Research Establishment, Suffield, Ralston (Alberta), Canada. (DRES-MEMO-25/68.)

Broekstra, G., *Note on Detonation and Blast Wave Theory, Part I, Detonation Theory*. Defence Research Establishment, Suffield, Ralston (Alberta), Canada. (DRES-MEMO-24/68.)

Dehn, James T., *Thermal Effects Which May Result in the Unexpected Ignition of Gaseous Mixtures*. Ballistic Research Laboratory, Aberdeen Proving Ground, Maryland, BRL-MR-2179.

Fullford, D. J., *Fuel Tank Inerting by Fuel Mist*. Royal Aircraft Establishment, Farnborough, England, RAE-TR-71175.

Keefer, John H., *Air Blast Predictions for Operation Distant Plain*. Ballistic Research Laboratory, Aberdeen Proving Ground, Maryland, BRL-TN-1612.

Lee, John H., Romas Knystautas, and Glen G. Bach. *Theory of Explosions*. McGill University, Montreal, Quebec, Department of Mechanical Engineering (MERL-69-10).

Lieb, Donald F., *An Exploratory Analysis of the Transition of Flash to Fuel Fire*. Ballistic Research Laboratory, Aberdeen Proving Ground, Maryland, BRL-1585.

Miller, R. E., and S. Wilford, *Simulated Crash Fire Tests As a Means of Rating Aircraft Safety Fuels*. Royal Aircraft Establishment, Farnborough, England, RAE-TR-71130.

Newman, M. M., and J. D. Robb, *Aircraft Protection From Thunderstorm Electromagnetic Effects, Part III, Fuel Vents - Special Effects*. Lightning and Transients Research Institute, Minneapolis, Minnesota.

Nowack, Clarence J., *Development of an Aircraft Fuel Additive to Suppress the Bulk Flammability of Fuel*. Naval Air Propulsion Test Center, Philadelphia, Pennsylvania, NAPT-C-AED-1903.

Parker, William J., R. C. Corlett and Billy T. Lee. *An Experimental Test of Mass Fire Scaling Principles*. Naval Radiological Defense Laboratory, San Francisco, Calif., USNRDL-TR-68-117.

Sakura, Akira, *Blast Wave Theory*. Wisconsin University, Madison, Mathematics Research Center, MRC-TSR-497.

Slutsky, Simon, Wallace Chinitz, T. Baurer, and J. Tamagno, *An Investigation of Hydrocarbon Combustion Kinetics in Supersonic Flows*. General Applied Science Labs., Inc., Westbury, New York, GASL-TR-541-A.

Wiggins, E. W. and O. Malmberg, *Aircraft Fuel Tank Inerting by Means of Fuel Cell Fuel Fogging*. McDonnell Aircraft Company, St. Louis, Missouri, Power and Fluid Systems Department (Contract F33615-68-C-1660).

Yallop, H. J., *The Investigation into the Causes of the Explosion at Ronan Point 16 May 1968*. Royal Armament Research and Development Establishment, Fort Halstead, England, RARDE-3/69.

## BLAST EFFECTS

Andersen, W. H., *Water Particle Pick-up and Acceleration in a Blast Wave Propagating Over a Water Surface*. Shock Hydrodynamics, Inc., (Contract N60921-67-C-0003).

Chan, B. C., M. Holt, and R. L. Welsh. *Explosions Due to Pressurized Spheres at the Ocean Surface*. University of California, Berkeley, ITS Report No. AS-66-11.

Cohen, E. A., *CCAMIN, A Computer Program for Fitting Time of Arrival and Shock Peak Over-Pressure Data in a Gas*. Naval Ordnance Laboratory, NOL-TR-71-169.

- Collins, R., *Intense Explosions at the Ocean Surface*. University of California, Berkeley, ITS Report No. AS-66-9.
- Ethridge, H. H., *A Suggested Plotting Procedure for Blast Parameters*. Ballistic Research Laboratory, APG, BRL-MR-1807.
- Forrestal, M. J. and M. R. Johnson, *Modified Atmosphere Effects on Air Blast and Ground Motion*. General American Transportation Corporation, ITS MR-1274.
- Fugelso, L. E., and S. F. Fields, *Dial Pack Blast Directing Experiment - Project LN 105*. General American Transportation Corporation, ITS GARD-1506.
- Goresch, J. W. and R. G. Dunn, *Tables of Blast Wave Parameters, I, Spherical Explosions*. Aerospace Research Laboratories, ARL-69-0011.
- High, R. W., *Some Liquid Oxygen, Liquid Hydrogen Explosive Effects in Controlled Failure-Mode Tests*. National Aeronautics and Space Administration, NASA TN-D-5382.
- Huffington, N. J. and J. D. Wortman, *An Analytical Study of Explosive Loading Techniques for Simulation of Impulsive Loading of Structures at Lethality Levels*. Ballistic Research Laboratory, APG, BRL-R-1621.
- Hurst, W. M., *Foil Gages for Measuring the Peak Pressures From Detonators in Air*. New Mexico Institute of Mining and Technology, ITS R-T-961.
- Johnson, M. R. and M. J. Balcerzak, *Modified Atmosphere Effects on Air Blast Project 1.09, Operation Distant Plain*. General American Transportation Corporation.
- Keefer, J. H. and J. D. Day, *Terrain Effects on Blast Wave Parameters*. Ballistic Research Laboratory, APG, BRL-TR-1319.
- Kinney, G. F., *Blast Wave Yields for an Explosion*. Naval Weapons Center, China Lake, Calif., NWC TP 5020.
- Kurz, F. R. and M. J. Balcerzak, *A Theoretical Investigation of Gas-Augmented High Explosive Simulation Technique*. General American Transportation Corporation, ITS MR-1274-600.
- Letho, D. L. and R. A. Larson, *Long Range Propagation of Spherical Shock Waves From Explosions in Air*. Naval Ordnance Laboratory, NOL-TR-69-88.
- Lucole, S. W. and M. J. Balcerzak, *High Yield Detonable Gas Explosions - Sledge Technique*. General American Transportation Company, ITS MR-1454.
- Morton, H. S., *Scaling the Effects of Air Blast on Typical Targets*. Applied Physics Laboratory, John Hopkins University, TG-733.

Pinkston, J. M. and A. Sakurai, *Water Shock Waves From Above-Water Explosions*. Waterways Experiment Station, Vicksburg.

Porzel, F. B., *Introduction to a Unified Theory of Explosives (UTE)*. Naval Ordnance Laboratory, NOL-TR-72-209.

Reisler, R. E., N. H. Ethridge, D. P. Lefevre, and L. Giglio-Tos, *Air Blast Measurements From the Detonation of an Explosive Gas Contained in a Hemispherical Balloon (Operation Distant Plain, Event 2A)*. Ballistic Research Laboratory, APG, BRL-MR-2108.

Ruetenik, J. R. and S. D. Lewis, *Pressure Probe and System for Measuring Large Blast Waves*. Massachusetts Institute of Technology, Aeroelastic and Structures Research Laboratory, ITS Tech Report 105-2.

Sakurai, A. and J. M. Pinkston, *Water Shock Waves Resulting From Explosions Above an Air-Water Interface - Results of a Theoretical Investigation*. Waterways Experiment Station, Vicksburg, ITS TR-1-771, R-1.

Schlueter, S. D., R. G. Hippensteel, and B. F. Armendt, *Measurements of Air Blast Parameters Above a Reflecting Surface*. Ballistic Research Laboratory, APG, ITS Memo Report 1645.

Wilton, C. and B. Gabrielson, *House Damage Assessment*. URS Research Company, ITS URS-788-5.

Wilton, C., *Assessments of House Damage From Event Dial Pack and 100 Ton AN FO Test*. URS Research Company, ITS URS-788-2.